Harnessing the immunostimulatory properties of oncolytic reovirus for anticancer immunotherapy

Groeneveldt, P.C.

CHAPTER 7

Intertumoral differences dictate the outcome of TGF-β blockade on the efficacy of viro-immunotherapy

Christianne Groeneveldt[1], Jurriaan Q. van Ginkel[1], Priscilla Kinderman[2], Marjolein Sluijter[1], Lisa Griffioen[1], Camilla Labrie[1], Diana J. M. van den Wollenberg[3], Rob C. Hoeben[3], Sjoerd H. van der Burg[1], Peter ten Dijke[4], Lukas J. A. C. Hawinkels[2], Thorbald van Hall[1], Nadine van Montfoort[2#]

[1] Department of Medical Oncology, Oncode Institute, Leiden University Medical Center, 2333 ZA, Leiden, The Netherlands

[2] Department of Gastroenterology and Hepatology, Leiden University Medical Center, 2333 ZA, Leiden, The Netherlands

[3] Department of Cell and Chemical Biology, Leiden University Medical Center, 2300 RC, Leiden, The Netherlands

[4] Department of Cell and Chemical Biology, Oncode Institute, Leiden University Medical Center, 2300 RC, Leiden, The Netherlands

[#] Corresponding author

Cancer Research Communications 2023;3(2):325–337

ABSTRACT

The absence of T cells in the tumor microenvironment of solid tumors is a major barrier to cancer immunotherapy efficacy. Oncolytic viruses, including reovirus type 3 Dearing (Reo), can recruit $CD8^+$ T cells to the tumor and thereby enhance the efficacy of immunotherapeutic strategies that depend on high T-cell density, such as CD3-bispecific antibody (bsAb) therapy. Transforming growth factor-β (TGF-β) signaling might represent another barrier to effective Reo&CD3-bsAb therapy due to its immunoinhibitory characteristics. Here, we investigated the effect of TGF-β blockade on the antitumor efficacy of Reo&CD3-bsAb therapy in the preclinical pancreatic KPC3 and colon MC38 tumor models, where TGF-β signaling is active. TGF-β blockade impaired tumor growth in both KPC3 and MC38 tumors. Furthermore, TGF-β blockade did not affect reovirus replication in both models and significantly enhanced the Reo-induced T-cell influx in MC38 colon tumors. Reo administration decreased TGF-β signaling in MC38 tumors but instead increased TGF-β activity in KPC3 tumors, resulting in the accumulation of αSMA^+ fibroblasts. In KPC3 tumors, TGF-β blockade antagonized the antitumor effect of Reo&CD3-bsAb therapy, even though T-cell influx and activity were not impaired. Moreover, genetic loss of TGF-β signaling in $CD8^+$ T cells did not affect therapeutic responses. In contrast, TGF-β blockade significantly improved therapeutic efficacy of Reo&CD3-bsAb in mice bearing MC38 colon tumors, resulting in a 100% complete response. Further understanding of the factors that determine this inter-tumor dichotomy is required before TGF-β inhibition can be exploited as part of viro-immunotherapeutic combination strategies to improve their clinical benefit.

Significance: Blockade of the pleiotropic molecule TGF-β can both improve or impair the efficacy of viro-immunotherapy, depending on the tumor model. While TGF-β blockade antagonized Reo&CD3-bsAb combination therapy in the KPC3 model for pancreatic cancer, it resulted in 100% complete responses in the MC38 colon model. Understanding factors underlying this contrast is required to guide therapeutic application.

GRAPHICAL ABSTRACT

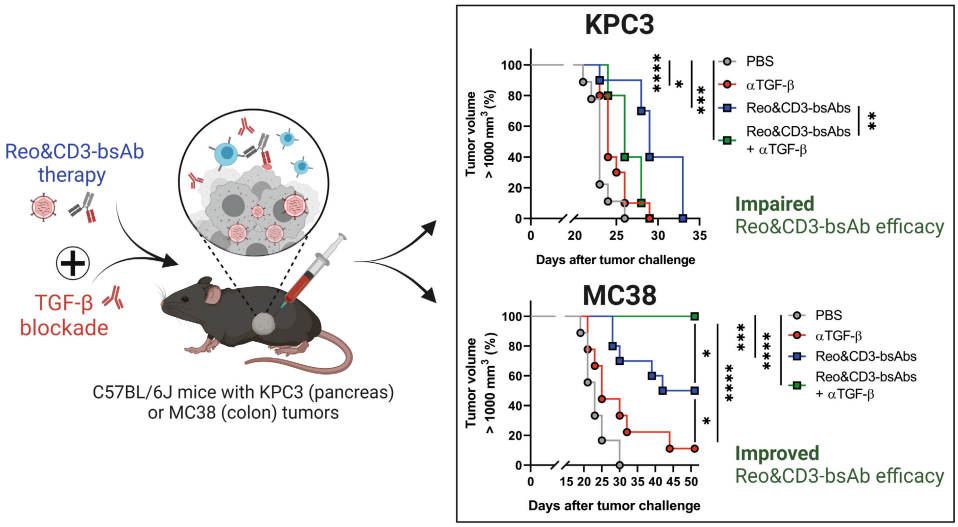

INTRODUCTION

Oncolytic viruses (OVs) are increasingly recognized as potent anticancer agents due to their preferential infection of cancerous cells and stimulation of host antitumor immunity (1). The mammalian reovirus type 3 Dearing strain (T3D) is one of the most prominent oncolytic viruses under clinical evaluation and displays an excellent safety record in clinical trials (2,3). Reoviruses show an inherent preference for replication in and lysis of transformed, but not healthy cells (4). Although reovirus has demonstrated moderate antitumor efficacy as monotherapy (5,6), studies have shown that its potential might be better utilized as a part of combinatorial approaches (7). For example, we recently demonstrated that sensitizing the tumor microenvironment (TME) of murine pancreatic KPC3 tumors with reovirus significantly enhanced the efficacy of otherwise non-effective CD3-bispecific antibodies (CD3-bsAbs). This enhanced efficacy could be attributed to the capability of reovirus to induce a fast interferon response which was followed by a potent influx of $CD8^+$ T cells (8). Others have shown that reovirus can sensitize the TME for immune checkpoint inhibition by enhancing the intratumoral density of tumor-specific $CD8^+$ T cells and upregulating immune checkpoint inhibitor Programmed Death-Ligand 1 (PD-L1) expression (9).

Although the use of OVs is very promising to attract T cells to solid tumors and improve the efficacy of immunotherapeutic strategies, these combination approaches rarely lead to complete cures. Various tumor types such as colorectal cancer, ovarian cancer, and pancreatic ductal adenocarcinoma (PDAC) (10-12) often present with high transforming growth factor-β (TGF-β) signaling, which might be another barrier to effective combinatorial immunotherapy (13-15). TGF-β acts as a tumor-promoting cytokine by stimulating cancer cell migration and invasion, extracellular matrix (ECM) remodeling, epithelial-to-mesenchymal transition (EMT), and the induction of an immunosuppressive TME (16). In particular, TGF-β acts as an immunosuppressive factor by inhibiting the generation and function of $CD4^+$ and $CD8^+$ effector T cells and dendritic cells (DCs), whilst promoting the expansion of regulatory T cells (Tregs) and myeloid-derived suppressor cells (17,18). Indeed, TGF-β blockade can promote the expansion of $CD8^+$ T cells, reduce the level of regulatory T cells (Tregs) and induce the polarization from pro-tumorigenic M2 macrophages to antitumor M1 macrophages (19,20).

Altogether, these observations hint towards a potential beneficial effect of TGF-β inhibition on the efficacy of immunotherapeutic strategies. For example, TGF-β inhibition has increased the efficacy of checkpoint blockade in mouse models for mammary carcinoma and metastatic breast cancer, and colorectal cancer (21-24). We hypothesized that the reovirus-induced increase in intratumoral T cells, combined with TGF-β inhibition to remove the immunosuppressive barrier in the TME, would also strongly enhance the efficacy of viro-immunotherapeutic strategies. In the present study, we investigated whether inhibition of TGF-β signaling further enhanced the

efficacy of reovirus and CD3-bispecific antibody therapy in preclinical tumor models with high TGF-β signaling.

MATERIAL & METHODS

Reovirus

The wild-type reovirus strain R124 (further referred to as Reo) was previously isolated from a heterogeneous reovirus Type 3 Dearing (T3D) stock (VR-824) obtained from the American Type Culture Collection (ATCC) by two rounds of plaque purification using HER911 cells (RRID:CVCL_1K15) (25). All experiments were performed using cesium chloride (CsCl)-purified stocks as described earlier (8). The total amount of particles was calculated based on OD_{260} values where 1 OD equals $2.10x10^{12}$ reovirus particles/mL, and the infectious titer was quantified by plaque assay on HER911 cells.

Cell lines and culture

The murine pancreatic cancer cell line KPC3 (RRID:CVCL_A9ZK) is a low-passage derivate of a primary KPC tumor with mutant *p53* and *K-ras* from a female C57BL/6 mouse (8,26). KPC3.TRP1 cells (RRID:CVCL_A9ZL) were generated as described (27) and selected for expression of tyrosine-related protein (TRP1) by cell sorting using an αTRP1 antibody (clone: TA99). The MC38 cell line (RRID: CVCL_B288) is a chemically-induced murine colon carcinoma. MC38.TRP1 cells were generated as described before for KPC3.TRP1 (27) by transfection of MC38 cells with a *TRP1/gp75*-coding plasmid using lipofectamine (Invitrogen) in a 1:3 ratio. Transfected cells were selected with 400 µg/mL geneticin (G418, ThermoFisher Scientific) and sorted twice for expression of TRP1 as described above. All cells were cultured at 37 °C in a humidified atmosphere containing 5% CO_2 in Iscove's Modified Dulbecco's Medium (IMDM; Invitrogen) supplemented with 8% fetal calf serum (FCS; Bodinco, Alkmaar, The Netherlands), 2 mM L-glutamine (Gibco), 100 µg/mL penicillin and 100 µg/mL streptomycin (Gibco). Cell lines were assured to be free of *Mycoplasma* by regular PCR analysis. Authentication of the cell lines was done by Short Tandem Repeat (STR) profiling (IDEXX BioAnalytics, Ludwigsburg, Germany) and cells of low passage number were used for all experiments.

Antibodies for in vivo administration

The CD3xTRP1 bispecific antibody (bsAb) used is a knob-into-hole bispecific based on murine IgG2a with an Fc Silent™ mutation, featuring one arm with an anti-mouse CD3e scFv based on the clone 145-2C11, and the other arm containing the TA99 clone directed against TRP1 (bAb0136; Absolute Antibody). Transforming growth factor-β (TGF-β) blockade was performed using the monoclonal TGF-β-blocking antibody (clone 1D11.16.8; InVivoMAb anti-mouse/human/rat/monkey/ hamster/canine/bovine TGF-β1, -2, -3; BioXCell).

Mouse experiments

Male C57BL/6J mice (RRID:IMSR_JAX:000664) (6-8 weeks old) were purchased from Charles River Laboratories (France). Male nonobese diabetic (NOD).Cg-Prkdc^{scid}Il2rg^{tm1Wjl}/SzJ (NSG) mice (RRID:IMSR_JAX:005557) (6-8 weeks old) were obtained from The Jackson Laboratory (Bar Harbor, Maine, USA). TGF-β receptor II (TβRII) knockout mice (TβRII$^{fl/fl}$) (28) were crossed with CD8a-driven Cre-knock-in mice (RRID:IMSR_JAX:008766) to generate CD8Cre$^{+/-}$TβRII$^{fl/fl}$ (CD8 TβRII KO) and CD8Cre$^{-/-}$TβRII$^{fl/fl}$ (TβRII WT) mice. Both male and female CD8 TβRII KO and TβRII WT mice (7-22 weeks old) were used in the experiment. Genomic PCR was conducted to analyze the genotypes of mice using ear DNA and gene-specific primers for the conditional TGF-βRII locus (28) and Cre construct (CRE transgene 5'-CAA TGG AAG GAA GTC GTG GT-3'; wt 5'-CAC ACA TGC AAG TCT AAA TCA GG-3'; CRE common 5'-TGG GAT TTA CAG GGC ATA CTG-3').

All mouse experiments were individually prepared, reviewed, ethically approved, and registered by the institutional Animal Welfare Body of Leiden University Medical Center and carried out under project license AVD1160020187004, issued by the competent authority on animal experiments in The Netherlands (named CCD: Centrale Commissie Dierproeven). Power calculation was performed to define optimal sample size. Experiments were performed following the Dutch Act on Animal Experimentation and EU Directive 2010/63/EU ("On the protection of animals used for scientific purposes") at the animal facility of the Leiden University Medical Center (LUMC), The Netherlands. Mice were housed in individually ventilated cages with no more than 5 mice/cage. After one week of acclimatization after transport, mice were inoculated in the right flank with subcutaneous KPC3(.TRP1) tumors ($1x10^5$ cells in 100 µL phosphate-buffered saline (PBS)/0.1% bovine serum albumin (BSA) or MC38(.TRP1) tumors ($5x10^5$ cells in 200 µL PBS/0.1% BSA). In the case of a rechallenge, mice that cleared the primary tumor were injected with the same number of cells in the alternate flank. Intratumoral reovirus administration was performed under isoflurane anesthesia by injection of $1x10^7$ plaque-forming units (pfu) of reovirus or PBS as a control in a volume of 30 µL PBS. Intravenous administration of reovirus after tumor challenge was performed by injection of $1x10^8$ pfu of reovirus in a total volume of 100 µL PBS in the tail vein. Treatment with CD3xTRP1 bsAbs consisted of 2-3 intraperitoneal (i.p.) injections of 12,5 µg antibody in 100 µL PBS, given every other day. αTGF-β was administered 2-3x/week by i.p. injections of 200 µg in 100 µL PBS.

Cages were randomly allocated to a certain treatment group by an independent researcher and treatments were given in a different order each time. During all experiments, tumors were measured 3-5 times a week in 3 dimensions using a caliper, in a blinded manner concerning the experimental group or genotype of the mice. For experiments where tumor growth was the experimental outcome, mice were sacrificed when the tumor volume exceeded 1000 mm^3. In the case where therapy response was determined: NR = no response; CR = complete response and PR = partial response (regression or constant tumor volumes for at least 7 days). For interim blood analysis,

blood was harvested by tail vein puncture. For intratumoral analysis experiments, mice were sacrificed at indicated days after treatment before tumors were collected. Tumors were divided into representative parts, which were either snap-frozen in liquid N2 and stored at -80 °C for further analysis or fixed in 4% formaldehyde (AddedPharma) for immunohistochemistry (see also **Supplementary Methods**). Alternatively, tumors were immediately processed to single cells suspensions for flow cytometry analysis.

Cell preparation and flow cytometry

Tumors were dissociated into a single-cell suspension as described before (8). Blood was incubated with red blood cell lysis buffer for 3 minutes at room temperature (RT) before use. Cells were incubated with Zombie AquaTM Fixable Viability Dye (BioLegend) in PBS at RT followed by incubation with 2.4G2 FcR blocking antibodies (clone 2.4G2; BD Biosciences) in FACS buffer (PBS, 0.5% BSA, and 0.2% NaN_3) for 20 minutes on ice. If applicable, cells were incubated with Reo $\mu1_{133\text{-}140}$ tetramer conjugated to APC or the Rpl18 tetramer conjugated to PE (both generated in-house) for 1 hour at RT in FACS buffer, after which surface markers (**Table S1**) were added directly to the tetramer mixture for 30 minutes of incubation at RT. For intracellular staining, cells were fixed and stained for transcription factors and nuclear proteins using the Foxp3 / Transcription Factor Staining Buffer Set (eBiosciences) according to the manufacturer's instructions. After completion of staining protocols, samples were fixed in 1% paraformaldehyde and acquired using a BD LSRFortessa™ X20 4L cell analyzer (BD Biosciences, San Jose, CA, USA) at the Flow cytometry Core Facility (FCF) of Leiden University Medical Center (LUMC) in Leiden, The Netherlands (https://www.lumc.nl/research/facilities/fcf). Data were analyzed using FlowJoTM Software Version 10 (Becton, Dickinson, and Company).

RNA isolation and RT-qPCR

A representative snap-frozen proportion (10-30 mg) of each tumor or organ was disrupted in lysis buffer (Promega) using a stainless bead and the TissueLyser LT (Qiagen). Total RNA of in vivo samples was using the ReliaPrep™ RNA Tissue Miniprep System (Promega) according to the manufacturer's protocol. Total RNA from in vitro samples was isolated from cell pellets using the NucleoSpin® RNA Kit (Macherey-Nagel™) according to the manufacturer's instructions. 500 ng of RNA was used to generate cDNA using the High-Capacity RNA-to-cDNATM Kit (ThermoFisher Scientific) according to the manufacturer's protocol. Reovirus genomic copies and expression levels of host genes (**Table S2**) in tumors were measured by RT-qPCR as previously described (8). Reovirus S4 copy numbers were determined based on a standard curve, generated with serial dilutions of plasmid pcDNA_S4. Log_{10} S4 copy numbers were calculated using a previously described formula (29). The expression of host genes was normalized to reference genes Mzt2 and Ptp4a2 using the Bio-Rad CFX Manager 3.1 Software (Bio-Rad).

Statistics

Sample size was calculated using the PS: Power and Sample Size Calculation program (Vanderbilt University, version 3.1.6) (30). For experiments where tumor growth was the experimental read-out, mice were excluded when tumor engraftment was not successful (1% of all tumor engraftments). For RT-qPCR analysis, samples were excluded when RNA concentration and/or sample purity were too low. For flow cytometry data, tumor samples were excluded when evidence for draining lymph node contamination was present. All graphs were prepared and statistical analyses were performed using the GraphPad Prism software (version 8.0.2) (RRID:SCR_002798). Statistical tests used for each figure are described in the figure legends. Significance levels are labeled with asterisks, with ns=non-significant, *p<0.05, **p<0.01, ***p<0.001, and ****p<0.0001.

RESULTS

Early blockade of TGF-β signaling delays tumor outgrowth of KPC3 and MC38 tumors

In our previous work, we demonstrated that preconditioning murine pancreatic KPC3 tumors with reovirus (Reo) potently sensitized these solid tumors for otherwise ineffective CD3-bispecific antibody (bsAb) therapy (abbreviated to Reo&CD3-bsAbs) (8). KPC3 tumors display many characteristics of human PDAC, including desmoplastic stroma containing α-smooth muscle actin ($\alpha SMA)^+$ fibroblasts and collagen, and the absence of $CD8^+$ T cells (**Figure 1A**). KPC3 tumors also display TGF-β signaling, as indicated by nuclear accumulation of epithelial and stromal phosphorylated Smad2, a signaling protein directly downstream of the TGF-β type I receptor. Similarly to the murine pancreatic KPC3 tumor model, murine colon MC38 tumors display phosphorylated Smad2, but they do not contain many αSMA^+ fibroblasts and collagen and show a basal presence of $CD8^+$ T cells (**Figure 1B**). Since TGF-β signaling is active in both KPC3 and MC38 tumor tumors (23) and TGF-β has many immunoinhibitory characteristics, we hypothesized that inhibition of TGF-β might enhance the efficacy of Reo&CD3-bsAb therapy in these models.

First, we assessed the effect of TGF-β blockade as a monotherapy. We employed the murine monoclonal antibody 1D11 (αTGF-β), which neutralizes all 3 isoforms of TGF-β (31). This antibody was effective in decreasing TGF-β signaling *in vitro*, as was determined using a transcriptional reporter assay (CAGA-Luciferase, **Figure S1A**) and phosphorylation of Smad2 (**Figure S1B**). We next assessed the effect of TGF-β inhibition *in vivo* by applying TGF-β blockade in immunocompetent mice bearing subcutaneous KPC3 or MC38 tumors. Interestingly, TGF-β blockade significantly delayed tumor outgrowth of both KPC3 and MC38 tumors, but only when TGF-β blockade was started early after tumor challenge (**Figure 1C, D**) and not when tumors were already established (**Figure S2A**). Especially in KPC3 tumors, this delay in tumor growth after early, but not late intervention with TGF-β blocking antibodies was accompanied by a decreased intratumoral collagen

deposition (**Figure 1E, F, Figure S2B**). The impaired outgrowth of KPC3 tumors after TGF-β blockade could not be attributed to a lower proliferation of tumor cells, since the frequency of Ki67^{+} cells was not affected (**Figure 1G**). Additionally, the same delay in KPC3 tumor growth after early TGF-β blockade could be observed in immunodeficient NSG mice that lack T, B, and NK cells, suggesting that this delay in tumor growth after TGF-β blockade is not immune-mediated (**Figure 1H**). Combined, these data demonstrate that early TGF-β blockade delays the outgrowth of both KPC3 and MC38 tumors, which could possibly lead to improved efficacy of Reo&CD3-bsAb therapy.

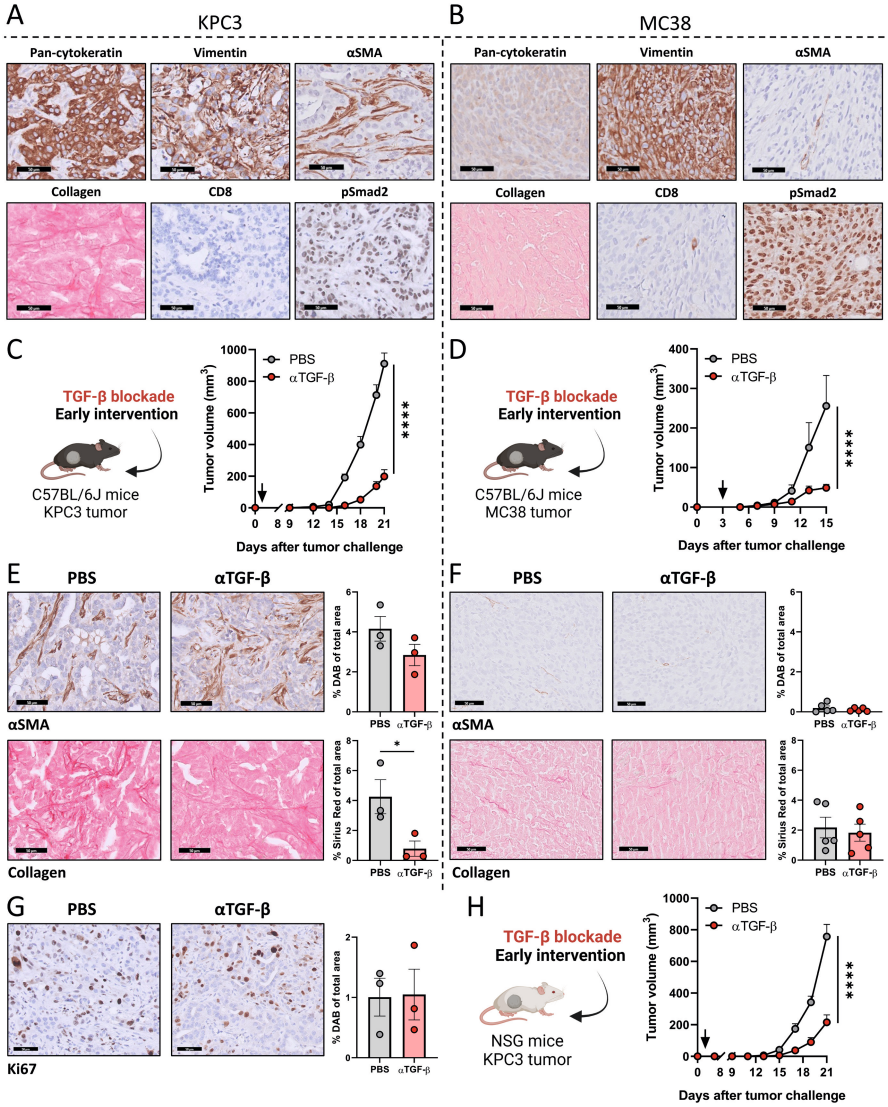

Figure 1. Early blockade of TGF-β signaling delays tumor outgrowth of KPC3 and MC38 tumors. (**A/B**) Representative images obtained from immunohistochemical (IHC) stainings of an untreated KPC3 (A) or MC38 (B) tumor for pan-cytokeratin, vimentin, smooth muscle actin-α (αSMA), collagen, CD8, and phosphorylated Smad2 (pSmad2). Scale bars equal 50 µm. >>

>> (**C/D**) Average tumor growth curves of immunocompetent KPC3 (C) or MC38 (D) tumor-bearing C57BL/6J mice (n=5/group) after TGF-β blockade. Mice were subcutaneously engrafted with KPC3 cells ($1x10^5$/mouse[5]) or MC38 cells ($5x10^5$/mouse) and received TGF-β-neutralizing antibodies (αTGF-β, 200 μg/injection every 3 days, starting from day 3 as indicated by the black arrow) as early intervention. (**E/F**) IHC stainings for αSMA and collagen in representative KPC3 (E) or MC38 (F) tumors after indicated treatments. Scale bars represent 50 μm and stainings were quantified using ImageJ. (**G**) IHC staining of Ki67 in KPC3 tumors treated with PBS or αTGF-β. Scale bars represent 50 μm and stainings were quantified using ImageJ. (**H**) Average tumor growth curves of immunodeficient KPC3-bearing NSG mice (n=8/group) after TGF-β blockade as early intervention, as described in (C). Data represent mean±SEM. Significance between PBS and αTGF-β in (E, F, G) was determined using unpaired t-tests. Significant differences in tumor growth between PBS and αTGF-β in (C, D, and H) were determined using an ordinary two-way analysis of variance (ANOVA) with Sidak's multiple comparisons test. Significance levels: *p<0.05 and ****p<0.0001.

TGF-β blockade does not impair Reo replication and the Reo-induced interferon response

Before investigating the effect of TGF-β blockade on the efficacy of Reo&CD3-bsAb therapy, we first analyzed whether TGF-β blockade would not affect the replication and immune-stimulatory properties of Reo in KPC3 and MC38 tumors. *In vitro,* Reo replication was not altered in KPC3 and MC38 cells after the addition of recombinant TGF-β or TGF-β inhibition (**Figure S3**). To confirm this *in vivo*, immunocompetent mice were treated with αTGF-β or left untreated and palpable tumors were injected with Reo. Reo replication and the Reo-induced expression of interferon-stimulated genes (ISGs) were compared between groups at the end of the experiment (**Figure 2A, B**). In both KPC3 and MC38 tumors, Reo replication (**Figure 2C, D**) and the Reo-induced expression of ISGs including T-cell-attracting chemokines *Cxcl9* and *Cxcl10* (**Figure 2E, F**) were not negatively affected after TGF-β blockade. Instead, the expression of various ISGs was higher in the groups that received Reo + αTGF-β compared to the group that received Reo only. Combined, these data indicate that TGF-β inhibition does not negatively influence the Reo-induced inflammatory response in the TME.

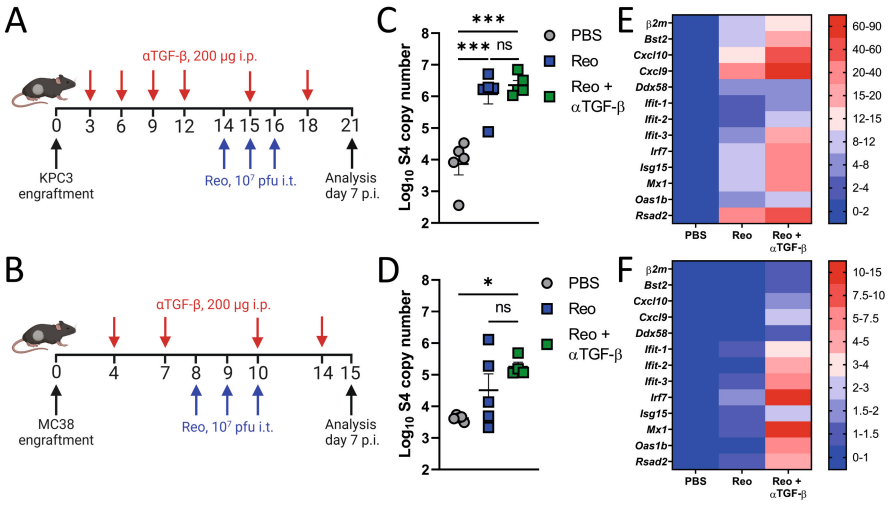

Figure 2. TGF-β blockade does not impair Reo replication and the Reo-induced interferon response in KPC3 and MC38 tumors. (**A**/**B**) Mice (n=4-5/group) were engrafted subcutaneously with KPC3 cells (1x10^5/mouse) (A) or MC38 cells (5x10^5/mouse) (B) and received TGF-β-neutralizing antibodies (αTGF-β, 200 μg/injection every 3 days) starting directly after tumor engraftment. Mice received Reo intratumorally on indicated days (10^7 plaque-forming units/injection)**.** Mice were sacrificed on day 21 (KPC3) or day 15 (MC38) for intratumoral analysis. (**C**/**D**) Reovirus genomic segment 4 (S4) copy number in KPC3 (C) or MC38 (D) tumor lysates, as determined by RT-qPCR. (**E**/**F**) Heatmap with relative expression of interferon response genes (ISGs) target genes in KPC3 (E) or MC38 (F) tumors after indicated treatments, as determined by RT-qPCR. Data represent mean±SEM. Significance between groups in (B) and (E) was determined using an ordinary two-way analysis of variance (ANOVA) with Tukey's post hoc test. Significance levels: ns=not significant, *p<0.05, ***p<0.001.

TGF-β blockade enhances the Reo-induced influx of T cells in MC38 tumors but not in KPC3 tumors

The efficacy of reovirus-based immunotherapy such as Reo&CD3-bsAb therapy relies on efficient Reo-induced intratumoral T-cell influx. Since TGF-β is known to promote an immunosuppressive and T-cell-excluding environment in the TME, we hypothesized that TGF-β blockade might further enhance the Reo-induced T-cell influx and function in these tumors. In KPC3 tumors, TGF-β blockade did not enhance the influx of total CD45$^+$ immune cells (**Figure 3A**) but significantly increased the frequency of NK cells after Reo administration (**Figure 3B**). Surprisingly, however, TGF-β blockade did not improve the Reo-induced influx of (reovirus-specific) CD8$^+$ T cells, nor their activation status (**Figure 3C-E**). TGF-β blockade also did not enhance total CD45$^+$ immune cell influx in MC38 tumors (**Figure 3F**), and again significantly improved the frequency of NK cells (**Figure 3G**).

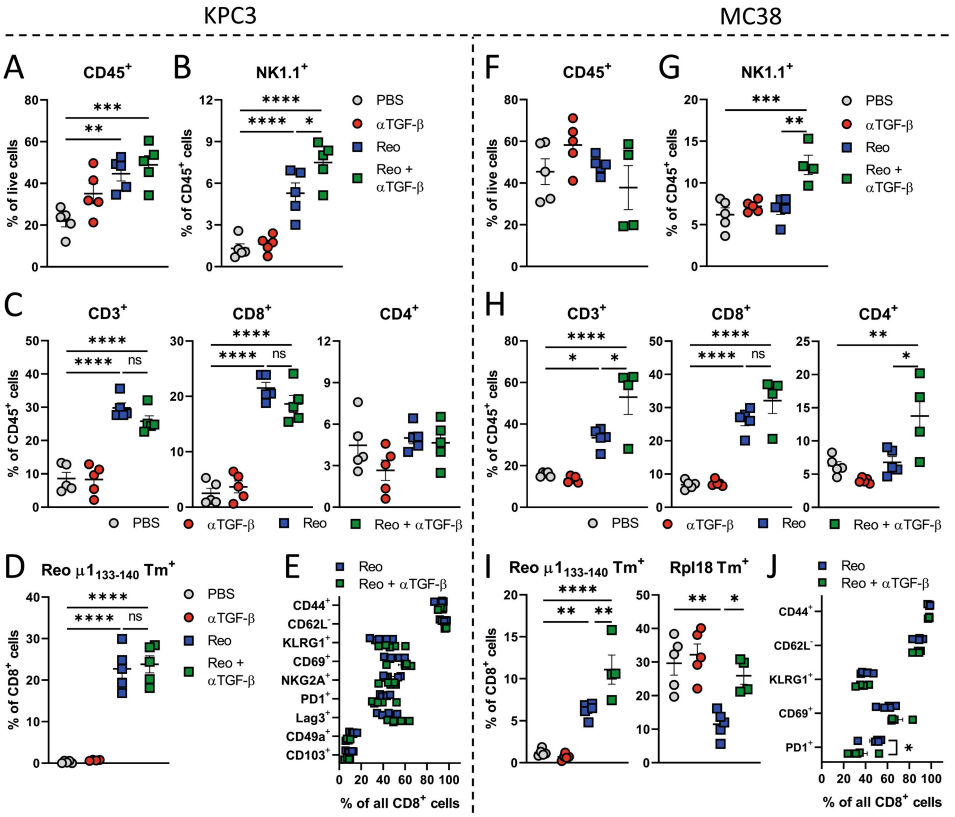

Figure 3. TGF-β blockade enhances the Reo-induced influx of T cells in MC38 tumors but not in KPC3 tumors. Experiments were performed according to the design described before in Figure 2A (KPC3) and Figure 2B (MC38). (**A**) Frequency of CD45$^+$ immune cells in KPC3 tumors after indicated treatments. (**B**) Frequency of NK cells within the CD45$^+$ immune cell population in KPC3 tumors. (**C**) Percentage of CD3$^+$, CD8$^+$, and CD4$^+$ T cells within CD45$^+$ immune cells in KPC3 tumors. (**D**) Frequency of reovirus-specific $\mu1_{133-140}$ T cells within the intratumoral CD8$^+$ T-cell population. (**E**) Expression of various markers on intratumoral CD8$^+$ T cells after receiving Reo only or Reo + αTGF-β. (**F**) Frequency of CD45$^+$ immune cells in MC38 tumors after indicated treatments. (**G**) Frequency of NK cells within the CD45$^+$ immune cell population in MC38 tumors. (**H**) Percentage of CD3$^+$, CD8$^+$, and CD4$^+$ T cells within CD45$^+$ immune cells in MC38 tumors. (**I**) Frequency of reovirus-specific $\mu1_{133-140}$ and tumor-specific Rpl18 T cells within the intratumoral CD8$^+$ T-cell population. (**J**) Expression of various markers on intratumoral CD8$^+$ T cells after receiving Reo only or Reo + αTGF-β. Data represent mean±SEM. Significance in (A-D) and (F-I) was determined using an ordinary one-way ANOVA with Tukey's multiple comparisons test. Significance between groups in (E) and (J) was determined using an ordinary two-way analysis of variance (ANOVA) with Tukey's post hoc test. Significance levels: ns=not significant, *p<0.05, **p<0.01, ***p<0.001 and ****p<0.0001.

Compared to KPC3 tumors, PBS-treated MC38 tumors already contained a higher basal frequency of $CD8^+$ T cells (6.808±0.57 vs 2.502±0.92) within the $CD45^+$ immune cell population. In contrast to KPC3 tumors, αTGF-β administration significantly increased the Reo-induced influx of total T cells in MC38 tumors (**Figure 3H**), as well as the frequency of reovirus-specific ($\mu1_{133\text{-}140}$ Tm^+) and tumor-specific (Rpl18 Tm^+) $CD8^+$ T cells compared to the group that received Reo only (**Figure 3I**). Expression of various activation markers on $CD8^+$ T cells was again comparable between both Reo-treated groups (**Figure 3J**). Combined, these data indicate that TGF-β blockade does not improve the Reo-induced T-cell influx and activation in KPC3 tumors. However, in MC38 tumors the frequency of T cells in the tumor, including reovirus- and tumor-specific T cells, is significantly enhanced when TGF-β signaling is inhibited.

Reovirus administration increases TGF-β signaling in KPC3, but not MC38 tumors

Next, we explored whether Reo administration affects TGF-β signaling in these tumors. Interestingly, when Reo was administered to mice bearing KPC3 tumors, a further increase in the presence of TGF-β1 levels in the tumor was observed (**Figure 4A**). Expression of various TGF-β target genes was also elevated within the tumor lysate (**Figure 4B**). Furthermore, Reo-treated tumors contained more αSMA-positive fibroblasts (**Figure 4C, D**), which are known to be induced by TGF-β (32). Together, these data suggest that TGF-β signaling is increased in KPC3 tumors after Reo administration, which provides an additional rationale to apply TGF-β blockade in combination with Reo-based viro-immunotherapy. In contrast, MC38 tumors displayed much lower total and active TGF-β1 levels in the tumor compared to KPC3 tumors, and the presence of active TGF-β was not increased upon Reo administration (**Figure 4E**). Additionally, expression of TGF-β target genes was decreased in Reo-treated MC38 tumors (**Figure 4F**) and the intratumoral presence of αSMA-positive fibroblasts was not increased (**Figure 4G, H**). We conclude that Reo differentially impacts TGF-β signaling in KPC3 and MC38 tumors, which might influence the added value of TGF-β blockade on the efficacy of Reo&CD3-bsAbs in these preclinical models.

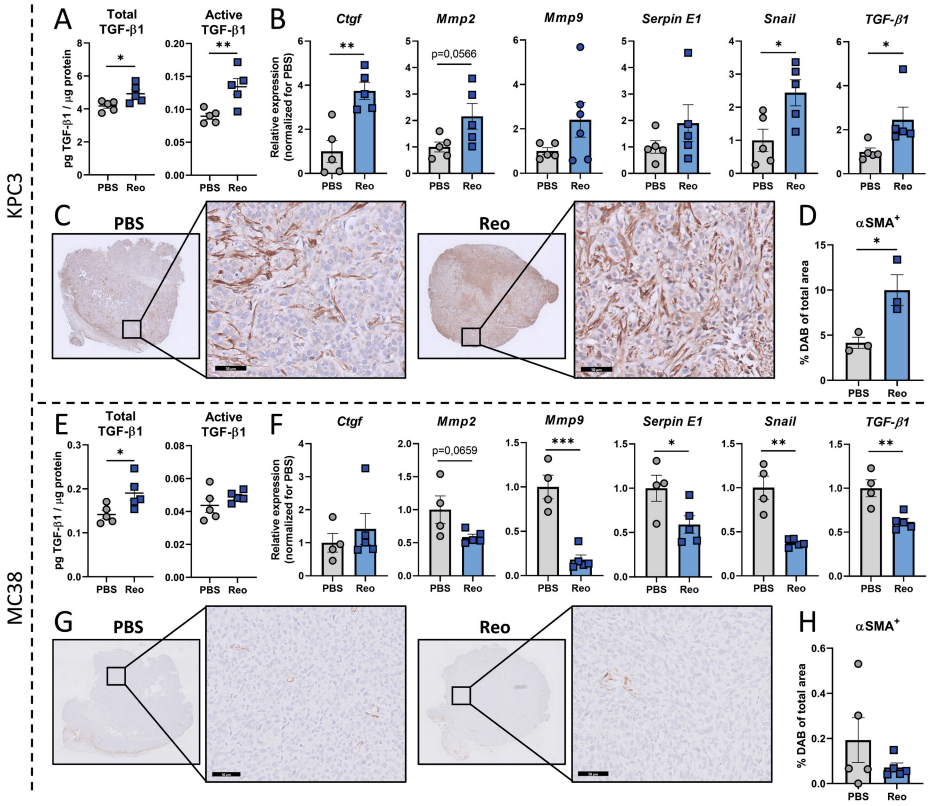

Figure 4. Reovirus administration increases TGF-β signaling in KPC3, but not MC38 tumors. (**A**) Levels of active and total TGF-β in tumor lysates of KPC3 tumors (n=4-5/group), treated intratumorally with PBS or Reo (3x 10^7 plaque-forming units) and harvested after 5 days. (**B**) Relative expression of TGF-β target genes in PBS- or Reo-treated KPC3 tumors (n=4-5/group), as determined by RT-qPCR. (**C**) Representative images obtained from immunohistochemical staining of PBS- or Reo-treated KPC3 tumors (n=3-5/group) for αSMA. Scale bars of magnification images equal 50 µm. (**D**) Quantification of positive DAB signal in sections stained for αSMA. (**E**) Levels of active and total TGF-β in tumor lysates of MC38 tumors (n=4-5/group), treated intratumorally with PBS or Reo (3x 10^7 plaque-forming units) and harvested after 5 days. (**F**) Relative expression of TGF-β target genes in PBS- or Reo-treated MC38 tumors (n=4-5/group), as determined by RT-qPCR. (**G**) Representative images obtained from immunohistochemical staining of PBS- or Reo-treated MC38 tumors (n=3-5/group) for αSMA. Scale bars of magnification images equal 50 µm. (**H**) Quantification of positive DAB signal in sections stained for αSMA. Data represent mean±SEM. Significance between PBS and Reo in (A, B), (D, E), and (H) was determined using unpaired t-tests. Significance levels: *p<0.05, **p<0.01 and ***p<0.001.

TGF-β blockade diminishes the efficacy of Reo&CD3-bsAb therapy in the pancreatic KPC3.TRP1 tumor model

We first employed the KPC3 tumor model to test our hypothesis that TGF-β blockade could improve the antitumor efficacy of Reo&CD3-bsAbs therapy. Immunocompetent mice were engrafted with a KPC3 tumor expressing tyrosine related protein 1 (TRP1) as a model antigen to be targeted by CD3-bsAbs (**Figure 5A**). As previously reported (8), Reo&CD3-bsAbs therapy induced steep regressions (**Figure 5B, C**), followed by tumor escape. Unexpectedly, however, TGF-β blockade did not improve Reo&CD3-bsAb therapy but abrogated its antitumor efficacy. Tumors of mice that received Reo&CD3-bsAbs as well as TGF-β blockade did not regress in size after receiving CD3-bsAbs but displayed similar tumor growth as observed in mice treated with TGF-β blockade alone (**Figure 5C, D**). Ultimately, Reo&CD3-bsAbs + αTGF-β treated mice did have significantly better survival compared to untreated mice, but their survival was significantly worse compared to mice that received Reo&CD3-bsAbs without TGF-β inhibition (**Figure 5E**).

The impaired efficacy of Reo&CD3-bsAbs, when combined with TGF-β blockade, could not be attributed to a lower presence of T cells, since tumors that received this triple combination therapy did not demonstrate lower intratumoral T-cell frequencies compared to the group that received Reo&CD3-bsAbs without αTGF-β (**Figure S4A**). Instead, there was a trend towards a higher T-cell presence in tumors after TGF-β blockade and Reo&CD3-bsAb therapy compared to the group that only received Reo&CD3-bsAb therapy, mimicking the increased T-cell influx after TGF-β blockade that was observed in MC38 tumors (**Figure 3H**). Expression levels of various T-cell activation markers were also similar between both groups (**Figure S4B**). Histological analysis confirmed that tumors of the Reo&CD3-bsAbs + αTGF-β group contained a high number of $CD3^+$ T cells that were spread throughout the whole tumor (**Figure S4C, D**). These data indicate that TGF-β inhibition did not impair the reovirus-induced quantity or location of effector T-cells in these end-stage KPC3.TRP1 tumors.

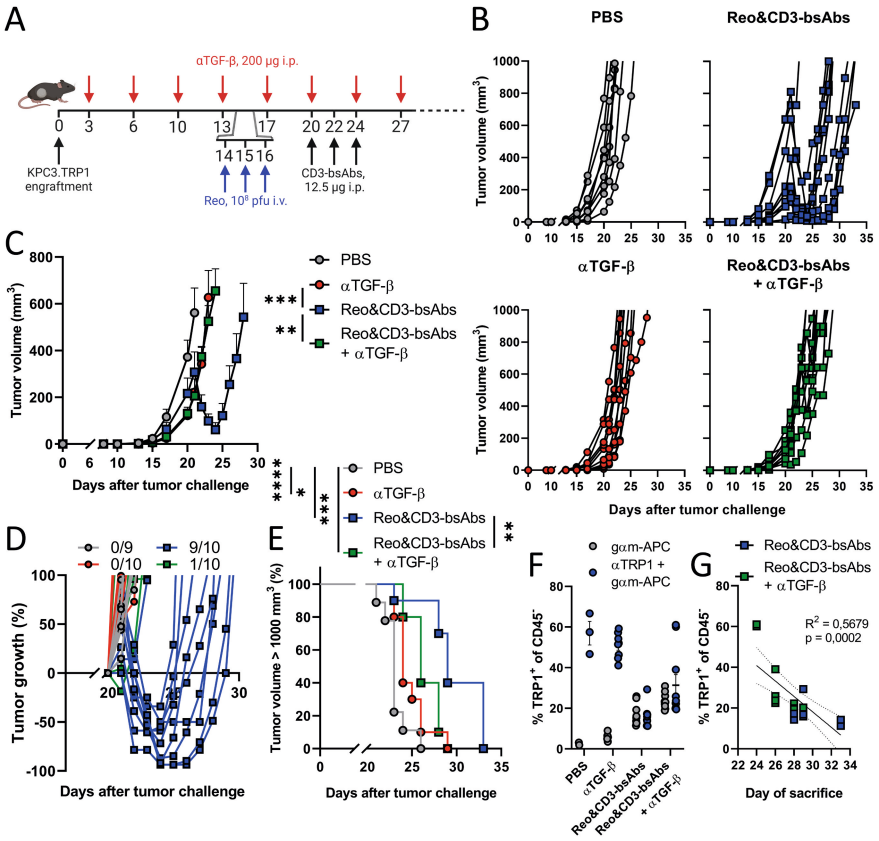

Figure 5. TGF-β blockade diminishes the efficacy of Reo&CD3-bsAb therapy in the KPC3.TRP1 tumor model. (**A**) Overview of the experiment described in (B-G). Mice (n=9-10/group) were subcutaneously engrafted with KPC3.TRP1 cells (1x10^5/mouse) and received TGF-β-neutralizing antibodies (αTGF-β, 200 µg/injection every 3 days) starting directly after tumor engraftment. Mice received Reo intravenously on days 14, 15, and 16 (10^8 plaque-forming units/injection) and received CD3-bsAbs intraperitoneally (12.5 µg/injection) on days 20, 22, and 24. Tumor growth was measured 3-5x/week. (**B**) Individual tumor growth curves of mice receiving indicated treatments. (**C**) Average tumor growth curves of mice receiving indicated treatments. One non-responding mouse in the Reo&CD3-bsAbs group is excluded for clarity (see also (B)). Significant differences in average tumor growth were calculated on day 23. (**D**) Relative changes in tumor volume of individual mice, calculated from the start of CD3-bsAb treatment. Indicated is the number of mice with tumor regressions in each group. (**E**) Kaplan-Meier survival graphs of mice after indicated treatments. (**F**) Quantification of TRP1 expression on CD45$^-$ cells within the end stage KPC3.TRP1 tumors after indicated therapies. Grey values indicate corresponding background staining of secondary goat-anti-mouse antibody only. (**G**) Correlation between TRP1 expression in tumors and the day of sacrifice. Data represent mean±SEM. Significance in (C) was determined using an ordinary one-way ANOVA with Tukey's multiple comparisons test. Log-rank tests were used to compare differences in survival in (E). Significance levels: *p<0.05, **p<0.01, ***p<0.001 and ****p<0.0001.

Since the impaired response to Reo&CD3-bsAb therapy after TGF-β blockade could not be attributed to a lower frequency of T cells, we next investigated whether an impaired quality of T cells might explain this effect. $CD8^+$ T cells are the main effector cells that infiltrate into the tumor after reovirus administration and are employed by CD3-bsAbs (27). *In vitro* experiments showed that the CD3-bsAb-induced cytotoxic efficacy of naive $CD8^+$ T cells was not impaired when TGF-β was added or neutralized (**Figure S5A**). Similarly, T cells of CD8 TβRII KO mice that selectively lacked TGF-β signaling in their $CD8^+$ T cells demonstrated similar cytotoxic capacity as TβRII wild-type (WT) T cells (**Figure S5B**). To confirm this *in vivo*, TβRII WT or CD8 TβRII KO mice were inoculated with KPC3.TRP1 tumor cells and received Reo&CD3-bsAb therapy as described earlier (**Figure S5C**). Interestingly, the efficacy of Reo&CD3-bsAb therapy was similar in TβRII WT and CD8 TβRII KO mice, while again Reo&CD3-bsAb + αTGF-β therapy demonstrated decreased antitumor effects and survival (**Figure S5D, E**).

Further flow cytometry analysis of end-stage tumors that received Reo&CD3-bsAbs as well as TGF-β blockade confirmed that TGF-β did not affect T-cell function. Tumors of mice that received Reo&CD3-bsAbs + αTGF-β demonstrated loss of TRP1 expression in the majority of $CD45^-$ cells, similar to tumors of mice treated with Reo&CD3-bsAb (**Figure 5F**), a phenomenon previously described in mice with successful tumor regressions upon Reo&CD3-bsAb treatment (8). Indeed, TRP1 expression in these groups negatively correlated with survival time until the experimental endpoint (**Figure 5G**), indicating that the best clinical response was correlated with the highest loss of TRP1 expression. Importantly, αTGF-β alone did not decrease the number of TRP1-expressing $CD45^-$ cells, indicating that the decreased frequency of TRP1-expressing cells after Reo&CD3-bsAb + αTGF-β was due to active attack and T-cell mediated killing of TRP1-expressing cells, and not because TGF-β blockade simply decreases TRP1 expression. Altogether, these data indicate TGF-β blockade impairs the efficacy of Reo&CD3-bsAb therapy in the KPC3 tumor model, even though the intratumoral T-cell frequency and their cytotoxic capacity were not negatively affected by TGF-β signaling inhibition.

TGF-β blockade significantly enhances the efficacy of Reo&CD3-bsAb therapy in the MC38.TRP1 model of colon cancer

We next investigated whether TGF-β blockade could improve the efficacy of Reo&CD3-bsAb therapy in the MC38 tumor model, which also displays high TGF-β signaling. Since MC38 tumor cells do not naturally express tumor antigen TRP1, we transfected MC38 cells with a plasmid encoding TRP1 and sorted $TRP1^+$ cells (**Figure S6A, B**), similar to what was previously done for KPC3. Hereafter, MC38.TRP1 cells were susceptible to T-cell mediated killing in the presence of CD3-bsAbs in an *in vitro* setting (**Figure S6C**), so we continued investigating whether TGF-β inhibition would improve the antitumor efficacy Reo&CD3-bsAb therapy in mice bearing MC38.TRP1 tumors (**Figure 6A**).

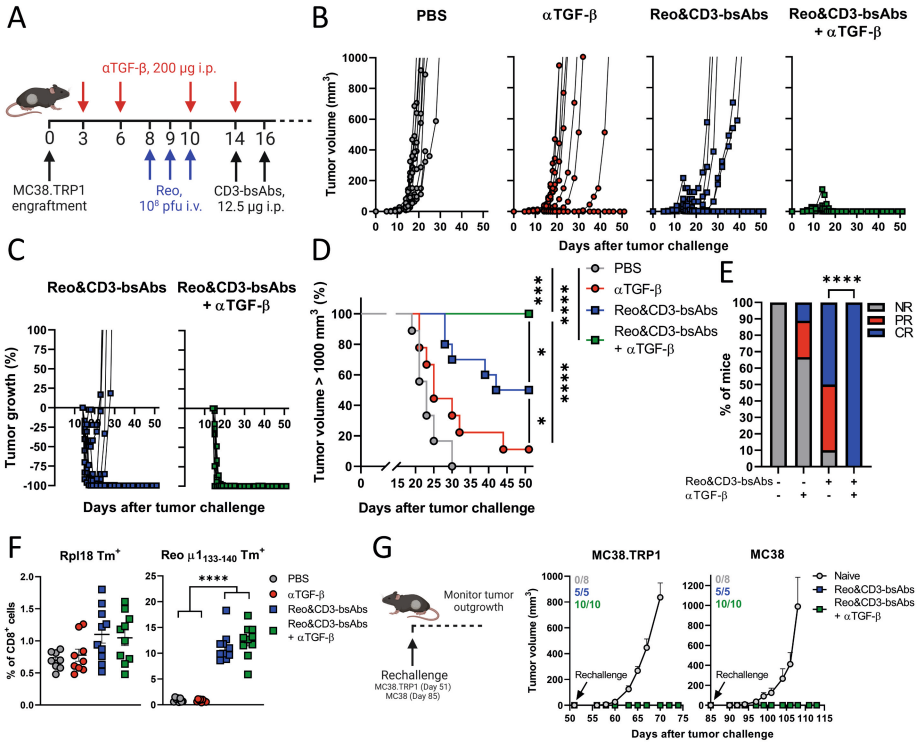

Figure 6. TGF-β blockade significantly enhances the efficacy of Reo&CD3-bsAb therapy in the MC38.TRP1 model of colon cancer. (**A**) Overview of the experiment described in (B-H). Mice (n=9-10/group) were subcutaneously engrafted with MC38.TRP1 cells (5x10^5/mouse) and received TGF-β-neutralizing antibodies (αTGF-β, 200 μg/injection every 3 days) starting directly after tumor engraftment. Mice received Reo (intravenously, 10^8 plaque-forming units/injection) and CD3-bsAbs (intraperitoneally, 200 μg/injection) on days 14 and 16. Tumor growth was measured 3x/week. (**B**) Individual tumor growth curves of mice receiving indicated treatments. (**C**) Relative changes in tumor volume of individual mice from the start of CD3-bsAb treatment. (**D**) Kaplan-Meier survival graphs of mice after indicated treatments. (**E**) Frequency of Non-Responders (NR), Partial Responders (PR; tumor regression/stagnation for more than 7 days), or Complete Responders (CR) within indicated treatment groups. (**F**) Frequency of Rpl18$^+$ and Reo μ1$_{133\text{-}140}$ CD8$^+$ T cells in the blood of mice after indicated treatments. (**G**) Rechallenge experiment. All CR mice from (D) were subcutaneously engrafted with MC38.(TRP1) tumor cells (5x10^5/mouse) in the alternate flank on day 51 (MC38.TRP1) or day 85 (MC38) and tumor outgrowth was measured 3x/week. Indicated is the number of mice within each group that rejected the rechallenge. Data represent mean±SEM. Log-rank tests were used to compare differences in survival in (D). A chi-square test was used to determine statistical differences in response in (E). Significance between groups in (F) was determined using an ordinary one-way ANOVA with Tukey's multiple comparisons test. Significance levels: *p<0.05, **p<0.01, ***p<0.001 and ****p<0.0001.

TGF-β blockade alone already delayed the outgrowth of MC38 tumors and induced complete tumor clearance in 1 out of 9 animals (=11.1%) (**Figure 6B**). In this model, Reo&CD3-bsAb therapy led to durable responses with complete tumor clearance in 50% of the animals (**Figure 6B**). Most interestingly, however, was the observation that here the efficacy of Reo&CD3-bsAb therapy was significantly improved by TGF-β inhibition. TGF-β inhibition combined with Reo&CD3-bsAb therapy led to very rapid tumor clearance in 100% of animals and significantly enhanced survival (**Figure 6C-E**). This increase in therapeutic efficacy could not be attributed to an increased presence of tumor-specific (Rpl18 Tm^+) or reovirus-specific ($\mu1_{133\text{-}140}$ Tm^+) $CD8^+$ T cells in the circulation, since their frequencies were similar between the group that received Reo&CD3-bsAb therapy and the group that received additional αTGF-β therapy (**Figure 6F**).

Since 50% of mice that received Reo&CD3-bsAb therapy and 100% of mice that received Reo&CD3-bsAb therapy in combination with αTGF-β completely cleared their tumor, we wondered whether tumor-specific immunologic memory was established. All mice that cleared the first tumor received a rechallenge at the alternate flank with MC38. TRP1 tumor cells, which was rejected (**Figure 6G**). Similarly, a third rechallenge with the parental MC38 cell line was also rejected, suggesting the establishment of an effective antitumor memory immune response. Combined, these data indicate that Reo&CD3-bsAb therapy alone is already effective in clearing MC38 tumors and establishing antitumor immunity, but the addition of αTGF-β significantly increases the primary antitumor response.

Altogether, we demonstrated that the addition of TGF-β blockade has the potential to improve the efficacy of Reo&CD3-bsAb therapy, but this benefit depends on the tumor model used. Although both KPC3 and MC38 tumors display active TGF-β signaling, the therapeutic efficacy of Reo&CD3-bsAbs was only drastically improved when TGF-β signaling was inhibited in MC38 tumors and not in KPC3 tumors. This differential effect of TGF-β blockade during Reo&CD3-bsAb combination therapy was associated with a different effect of Reo on TGF-β signaling in these tumors. Further understanding of inter-tumor differences that might contribute to this differential effect of TGF-β blockade is essential to improve, and not impair, the efficacy of viro-immunotherapeutic strategies.

DISCUSSION

In this study, we demonstrated that the combination therapy of reovirus and CD3-bispecific antibodies (Reo&CD3-bsAbs) can be significantly improved by additional neutralization of TGF-β. However, the added benefit of TGF-β blockade is model-dependent. Our data indicate that inhibition of TGF-β signaling might be a promising

strategy to enhance the efficacy of viro-immunotherapeutic strategies, but inter-tumor differences might also result in the diminishing of their efficacy after TGF-β blockade. TGF-β is mostly recognized as a tumor-promoting cytokine by inducing cancer cell migration and invasion (33,34) and as an immunosuppressive factor by inhibiting the generation and effector function of $CD4^+$ and $CD8^+$ effector T cells (17). The tumor-promoting and immunoinhibitory characteristics of TGF-β make it an attractive target for therapeutic intervention to enhance the efficacy of (viro-)immunotherapeutic strategies.

In preclinical research, 1D11 is a well-known antibody that prevents the binding of TGF-β isoforms to TGF-b receptors (31). TGF-β blockade using 1D11 only induced suppression of tumor growth when TGF-β blockade was initiated directly after tumor challenge (early intervention), and not when αTGF-β treatment was initiated when tumors were already established (late intervention). Similar observations were made in an MDA-MB-231 model of bone metastasis, where the reduced tumor burden in the bones after TGF-β inhibition was much more pronounced when TGF-β blockade was administered directly after tumor inoculation, compared to administration when metastases in the bones were already established (35). Additionally, treatment of established, orthotopic MDA-MB-231 tumors with 1D11 did not impact tumor growth, while stable overexpression of a soluble TGF-βRII (i.e. continued neutralization of TGF-β) almost completely blocked the growth of the same tumor (36). For KPC3 tumors, the impaired tumor growth suppression after early TGF-β blockade was not immune-mediated and could not be associated with impaired proliferation, but was associated with decreased intratumoral collagen disposition, as has also been observed in the murine mammary carcinoma 4T1 model and the human mammary carcinoma MDA-MB-231 model (36,37). These combined observations suggest that the TGF-β blockade-induced delay in tumor growth might be a result of microenvironmental changes, rather than a direct effect on tumor cells.

In our studies, we observed that TGF-β inhibition using 1D11 did not improve the efficacy of Reo&CD3-bsAb therapy in the murine pancreatic KPC3 model, but did significantly enhance the number of responders and overall survival in the murine colon MC38 model. A similar contrast was observed in a study where TGF-β inhibition enhanced the efficacy of checkpoint blockade in the MC38 tumor model but was unable to do so in a model for murine pancreatic cancer (23). The divergent effects of TGF-β blockade have also been observed in a panel of 12 models for metastatic breast cancer, where TGF-β using 1D11 suppressed the formation of lung metastasis in 42% of the models, did not induce a response in 33% of the models and induced an increase in lung metastasis in 25% of the models (38). An understanding of the factors underlying this dichotomy would be a first step towards predicting which individuals would most likely benefit from TGF-β neutralization in addition to viro-immunotherapy.

First, we took a closer look at the composition of the TME in both tumors. One big difference between the tumor models used is the immunogenicity and the related baseline frequency of tumor-infiltrated immune cells. The chemically-induced MC38 tumor model is more immunogenic compared to the genetically-induced KPC3 tumor model. Higher immunogenicity is associated with higher therapeutic efficacy of TGF-β inhibition, as was observed in a study where TGF-β inhibition using kinase inhibitor galunisertib resulted in stronger $CD8^+$ T-cell dependent control of tumor growth of immunogenic 4T1-Luciferase breast tumors, compared to poorly immunogenic 4T1 parental tumors (39). Similarly, TGF-β blockade in multiple squamous cell carcinoma (SCC) models using the pan-TGF-β neutralizing antibody was most effective in SCC tumors with the highest mutational loads (19). Immunogenic MC38 tumors already contain more T cells at baseline compared to poorly immunogenic KPC3 tumors, and TGF-β inhibition was able to further enhance the reovirus-induced influx of T cells in MC38 tumors. Interestingly, previous studies indicated that the main mechanism of action of TGF-β blockade to improve the efficacy of checkpoint blockade is by increasing T-cell infiltration into the tumor (21,40). Our data suggest that this might also be valid for other immunotherapeutic strategies, including Reo&CD3-bsAb therapy.

Another difference between the TME of both tumor models is the abundance of stroma in KPC3 tumors, which is absent in MC38 tumors. The tumor stroma consists, amongst other components, of fibroblasts, matrix proteins, and the vasculature (41). The importance of tumor stroma for the development, promotion, and invasion of cancer has become increasingly clear. In particular, cancer-associated fibroblasts can stimulate the growth, invasion, angiogenesis, and metastasis of tumors (42). As such, various stroma-related factors, such as an abundance of αSMA^+ fibroblasts and high expression of fibroblast activation protein (FAP), are associated with aggressive disease progression, recurrence, and therapy resistance in pancreatic and colorectal cancer (43-46). Matrix proteins such as type I collagens can promote the proliferation and invasiveness of tumor cells (47,48). High collagen content and cross-linking also contribute to tumor stiffness and drive metastatic growth (49). Interestingly, collagen can also decrease responses to immunotherapy by acting as a physical barrier to immune cell infiltration, as well as delivering inhibitory signals to immune cells such as T and NK cells by binding to the leukocyte-associated immunoglobulin-like receptor-1 (LAIR-1) (50). Although TGF-β inhibition was able to decrease αSMA^+ fibroblast and collagen content in KPC3 tumors, this decrease might not have been sufficient to enhance the efficacy of Reo&CD3-bsAb therapy similarly as was observed in MC38 tumors where the stromal compartment is mostly absent.

Additionally, besides the difference in T-cell infiltration or stromal composition, tumor-intrinsic differences might explain the differential effects of TGF-β inhibition on therapy outcome. Both KPC3 and MC38 tumor models used in this study display active signaling of TGF-β. Canonical TGF-β signaling involves the formation of a heterooligomer complex comprising Smad4 and other Smad proteins, that travels to the nucleus to induce

expression of TGF-β target genes (51). Alternatively, TGF-β signaling can also occur non-canonically, in a Smad4-independent manner. While canonical TGF-β signaling is involved in both tumor-promoting and tumor-suppressive pathways, non-canonical TGF-β signaling especially activates tumor-promoting pathways that facilitate EMT and cell migration, such as the RAS/RAF/MEK/ERK pathway. Interestingly, unlike KPC3, MC38 cells do not display Smad4-dependent signaling, even though Smad2 is phosphorylated (52). This lack of Smad4 expression results in enhanced tumorigenicity and metastatic potential, which could be reduced when Smad4 was introduced in these cells (52). Thus, Smad4 loss might result in the uncoupling of the TGF-β-mediated growth-suppressive function from its pro-oncogenic effects (53), which might explain why especially in the MC38 model TGF-β inhibition was very effective. Indeed, ablation of Smad4 expression in murine pancreatic 6694c2 tumors enhanced T-cell influx and improved the response to chemo-immunotherapy (54). Since both canonical and non-canonical TGF-β signaling pathways are intact in the KPC3 model, TGF-β inhibition might not only lead to the inhibition of its tumor-promoting pathways but also some of its tumor-suppressive aspects. This is eloquently demonstrated in the murine pancreatic BMFA3 tumor model, where treatment with an anti-TGFβR2 antibody significantly slowed the growth of *Tgfbr2*-mutant tumors but increased the growth of *Tgfbr*^{wt} tumors (55).

Another difference that we found between both models was the contrasting effect of Reo on TGF-β signaling. We observed that Reo administration leads to a further elevated presence of TGF-β in KPC3 tumors, which was accompanied by an increased expression of various TGF-β target genes and αSMA^{+} fibroblasts. An increase in TGF-β production after Reo administration has also been observed in other tumor models, as well as after other OV infections (56-59). In contrast, Reo administration led to decreased TGF-β signaling in MC38 tumors. This may imply that in KPC3 tumors blockade of TGF-β signaling is overruled by reovirus administration, while in MC38 tumors TGF-β blockade works synergistically with the Reo-induced decrease in TGF-β signaling and thereby results in significantly improved antitumor responses in these tumors. However, these opposite effects of Reo administration on TGF-β production and the expression of TGF-β target genes may not necessarily involve the canonical TGF-β signaling pathway, since MC38 tumor cells lack Smad4-mediated responses and the expression of many TGF-β target genes can also be induced or inhibited by other pathways.

In conclusion, we demonstrated that TGF-β blockade can differentially affect the efficacy of Reo&CD3-bsAb therapy in different preclinical tumor models, even if both models display active TGF-β signaling at baseline. These opposite effects might be attributed to the baseline T-cell density, immunogenicity, stromal composition, genetic factors including Smad4 deficiency, the effect of TGF-β blockade on the reovirus-induced T-cell influx into the tumor, or the effect of reovirus administration on TGF-β signaling. Further understanding of these inter-model differences that dictate whether TGF-β blockade promotes or impairs viro-immunotherapy is needed to guide further therapeutic developments. Since both oncolytic virus-based immunotherapeutic strategies (60),

as well as several therapeutic approaches to inhibit TGF-β signaling (51), are in clinical development, the implications of this research may be valuable for clinical practice.

DECLARATIONS

Acknowledgments. The authors are grateful to Prof. Stefan Karlsson (Lund University Hospital, Sweden) for the TβRII floxed mice. The authors appreciate the technical assistance from Stef G. T. Janson regarding the Western Blotting and Eveline S. M. de Jonge-Muller regarding the immunohistochemistry stainings, as well as Gaby Schaap and Jim Middelburg for their assistance with generating the MC38.TRP1 cell line. The authors gratefully acknowledge the operators of the Flow cytometry Core Facility (FCF) of the LUMC and the Animal Facility of the LUMC for their excellent support and care of the animals, respectively. All figures regarding experimental designs are created with BioRender.com.

Author contributions. Conceptualization, C.G., L.J.A.C.H., T.v.H., N.v.M.; Methodology, C.G., J.Q.v.G., P.K., M.S., L.G., C.L., D.v.d.W, R.H., L.J.A.C.H., T.v.H., N.v.M.; Formal analysis, C.G.; Investigation, C.G., J.Q.v.G., P.K.; Resources, D.v.d.W., R.H., M.S., L.J.A.C.H., P.t.D.; Writing – Original Draft, C.G., N.v.M.; Writing - Review & Editing, C.G., P.t.D., L.J.A.C.H., S.H.v.d.B., T.v.H, N.v.M.; Visualization, C.G.; Supervision, N.v.M.; Funding acquisition, S.H.v.d.B., T.v.H., N.v.M.. All authors approved the final version of the manuscript.

Funding. This work was financially supported by the Dutch Cancer Society Bas Mulder Award 11056 (to NvM), a PhD fellowship from Leiden University Medical Center (to CG), and the Support Casper campaign by the Dutch foundation 'Stichting Overleven met Alvleesklierkanker' (supportcasper.nl) project number SOAK 17.04 (to SHvdB, TvH, and NvM). RCH received funding for the work on oncolytic reoviruses from the Dutch Research Council (NWO)/STW Biotechnology and Safety program for the project 'Environmental safety evaluation of host range-modified oncolytic viruses' (project number 15414). PtD received funding from the Cancer Genomics Centre Netherlands (CGC.nl) through the NWO 'Zwaartekracht' program. Authors CG, JQvG, MS, LG, CL, SHvdB, PtD, and TvH are affiliated with Oncode Institute, an independent institute dedicated to understanding cancer and translating research into practice. Oncode Institute receives funding from the Dutch Cancer Society and ZonMw.

Conflicts of Interest. The authors declare no conflict of interest. The funders had no role in the design of the study; in the collection, analyses, or interpretation of data; in the writing of the manuscript, or in the decision to publish the results.

Data Availability. The data generated in this study are available upon reasonable request from the corresponding author.

REFERENCES

1. Groeneveldt C, van Hall T, van der Burg SH, Ten Dijke P, van Montfoort N. Immunotherapeutic Potential of TGF-β Inhibition and Oncolytic Viruses. Trends Immunol **2020**;41:406-20
2. Mahalingam D, Goel S, Aparo S, Patel Arora S, Noronha N, Tran H*, et al.* A Phase II Study of Pelareorep (REOLYSIN(®)) in Combination with Gemcitabine for Patients with Advanced Pancreatic Adenocarcinoma. Cancers (Basel) **2018**;10:160
3. Sborov DW, Nuovo GJ, Stiff A, Mace T, Lesinski GB, Benson DM*, et al.* A Phase I Trial of Single-Agent Reolysin in Patients with Relapsed Multiple Myeloma. Clinical Cancer Research **2014**;20:5946-55
4. Phillips MB, Stuart JD, Rodríguez Stewart RM, Berry JT, Mainou BA, Boehme KW. Current understanding of reovirus oncolysis mechanisms. Oncolytic Virother **2018**;7:53-63
5. Zhao X, Chester C, Rajasekaran N, He Z, Kohrt HE. Strategic Combinations: The Future of Oncolytic Virotherapy with Reovirus. Molecular cancer therapeutics **2016**;15:767-73
6. Kicielinski KP, Chiocca EA, Yu JS, Gill GM, Coffey M, Markert JM. Phase 1 clinical trial of intratumoral reovirus infusion for the treatment of recurrent malignant gliomas in adults. Mol Ther **2014**;22:1056-62
7. Müller L, Berkeley R, Barr T, Ilett E, Errington-Mais F. Past, Present and Future of Oncolytic Reovirus. Cancers **2020**;12:3219
8. Groeneveldt C, Kinderman P, van den Wollenberg DJM, van den Oever RL, Middelburg J, Mustafa DAM*, et al.* Preconditioning of the tumor microenvironment with oncolytic reovirus converts CD3-bispecific antibody treatment into effective immunotherapy. J Immunother Cancer **2020**;8:e001191
9. Samson A, Scott KJ, Taggart D, West EJ, Wilson E, Nuovo GJ*, et al.* Intravenous delivery of oncolytic reovirus to brain tumor patients immunologically primes for subsequent checkpoint blockade. Sci Transl Med **2018**;10:eaam7577
10. Kortekaas KE, Santegoets SJ, Abdulrahman Z, van Ham VJ, van der Tol M, Ehsan I*, et al.* High numbers of activated helper T cells are associated with better clinical outcome in early stage vulvar cancer, irrespective of HPV or p53 status. Journal for ImmunoTherapy of Cancer **2019**;7:236
11. Galon J, Bruni D. Approaches to treat immune hot, altered and cold tumours with combination immunotherapies. Nature Reviews Drug Discovery **2019**;18:197-218
12. Soleimani A, Pashirzad M, Avan A, Ferns GA, Khazaei M, Hassanian SM. Role of the transforming growth factor-β signaling pathway in the pathogenesis of colorectal cancer. Journal of Cellular Biochemistry **2019**;120:8899-907
13. Shen W, Tao GQ, Zhang Y, Cai B, Sun J, Tian ZQ. TGF-beta in pancreatic cancer initiation and progression: two sides of the same coin. Cell & Bioscience **2017**;7:39
14. Chae YK, Chang S, Ko T, Anker J, Agte S, Iams W*, et al.* Epithelial-mesenchymal transition (EMT) signature is inversely associated with T-cell infiltration in non-small cell lung cancer (NSCLC). Scientific reports **2018**;8:2918
15. Ganesh K, Massagué J. TGF-β Inhibition and Immunotherapy: Checkmate. Immunity **2018**;48:626-8
16. Angioni R, Sánchez-Rodríguez R, Viola A, Molon B. TGF-β in Cancer: Metabolic Driver of the Tolerogenic Crosstalk in the Tumor Microenvironment. Cancers (Basel) **2021**;13
17. Batlle E, Massague J. Transforming Growth Factor-beta Signaling in Immunity and Cancer. Immunity **2019**;50:924-40
18. Nixon BG, Gao S, Wang X, Li MO. TGFβ control of immune responses in cancer: a holistic immuno-oncology perspective. Nature Reviews Immunology **2022**;doi.org/10.1038/s41577-022-00796-z

19. Dodagatta-Marri E, Meyer DS, Reeves MQ, Paniagua R, To MD, Binnewies M*, et al.* α-PD-1 therapy elevates Treg/Th balance and increases tumor cell pSmad3 that are both targeted by α-TGFβ antibody to promote durable rejection and immunity in squamous cell carcinomas. Journal for immunotherapy of cancer **2019**;7:10.1186/s40425-018-0493-9
20. Jiao S, Subudhi SK, Aparicio A, Ge Z, Guan B, Miura Y*, et al.* Differences in Tumor Microenvironment Dictate T Helper Lineage Polarization and Response to Immune Checkpoint Therapy. Cell **2019**;179:1177-90.e13
21. Mariathasan S, Turley SJ, Nickles D, Castiglioni A, Yuen K, Wang Y*, et al.* TGFbeta attenuates tumour response to PD-L1 blockade by contributing to exclusion of T cells. Nature **2018**;554:544-8
22. Vanpouille-Box C, Diamond JM, Pilones KA, Zavadil J, Babb JS, Formenti SC*, et al.* TGFbeta Is a Master Regulator of Radiation Therapy-Induced Antitumor Immunity. Cancer Res **2015**;75:2232-42
23. Sow HS, Ren J, Camps M, Ossendorp F, ten Dijke P. Combined Inhibition of TGF-β Signaling and the PD-L1 Immune Checkpoint Is Differentially Effective in Tumor Models. Cells **2019**;8
24. Terabe M, Robertson FC, Clark K, De Ravin E, Bloom A, Venzon DJ*, et al.* Blockade of only TGF-beta 1 and 2 is sufficient to enhance the efficacy of vaccine and PD-1 checkpoint blockade immunotherapy. Oncoimmunology **2017**;6:e1308616
25. van den Wollenberg DJM, Dautzenberg IJC, van den Hengel SK, Cramer SJ, de Groot RJ, Hoeben RC. Isolation of reovirus T3D mutants capable of infecting human tumor cells independent of junction adhesion molecule-A. PLoS One **2012**;7:e48064-e
26. Hingorani SR, Wang L, Multani AS, Combs C, Deramaudt TB, Hruban RH*, et al.* Trp53R172H and KrasG12D cooperate to promote chromosomal instability and widely metastatic pancreatic ductal adenocarcinoma in mice. Cancer cell **2005**;7:469-83
27. Benonisson H, Altıntaş I, Sluijter M, Verploegen S, Labrijn AF, Schuurhuis DH*, et al.* CD3-Bispecific Antibody Therapy Turns Solid Tumors into Inflammatory Sites but Does Not Install Protective Memory. Molecular cancer therapeutics **2019**;18:312-22
28. Levéen P, Larsson J, Ehinger M, Cilio CM, Sundler M, Sjöstrand LJ*, et al.* Induced disruption of the transforming growth factor beta type II receptor gene in mice causes a lethal inflammatory disorder that is transplantable. Blood **2002**;100:560-8
29. Mijatovic-Rustempasic S, Tam KI, Kerin TK, Lewis JM, Gautam R, Quaye O*, et al.* Sensitive and specific quantitative detection of rotavirus A by one-step real-time reverse transcription-PCR assay without antecedent double-stranded-RNA denaturation. Journal of clinical microbiology **2013**;51:3047-54
30. Dupont WD, Plummer WD, Jr. Power and sample size calculations. A review and computer program. Controlled clinical trials **1990**;11:116-28
31. Bedinger D, Lao L, Khan S, Lee S, Takeuchi T, Mirza AM. Development and characterization of human monoclonal antibodies that neutralize multiple TGFβ isoforms. MAbs **2016**;8:389-404
32. Hata S, Okamura K, Hatta M, Ishikawa H, Yamazaki J. Proteolytic and Non-proteolytic Activation of Keratinocyte-Derived Latent TGF-β1 Induces Fibroblast Differentiation in a Wound-Healing Model Using Rat Skin. Journal of Pharmacological Sciences **2014**;124:230-43
33. Massague J. TGFbeta in Cancer. Cell **2008**;134:215-30
34. Connolly EC, Freimuth J, Akhurst RJ. Complexities of TGF-beta targeted cancer therapy. Int J Biol Sci **2012**;8:964-78
35. Biswas S, Nyman JS, Alvarez J, Chakrabarti A, Ayres A, Sterling J*, et al.* Anti-transforming growth factor ß antibody treatment rescues bone loss and prevents breast cancer metastasis to bone. PloS one **2011**;6:e27090-e
36. Liu J, Liao S, Diop-Frimpong B, Chen W, Goel S, Naxerova K*, et al.* TGF-β blockade improves the distribution and efficacy of therapeutics in breast carcinoma by normalizing the tumor stroma. Proc Natl Acad Sci U S A **2012**;109:16618-23

37. Grauel AL, Nguyen B, Ruddy D, Laszewski T, Schwartz S, Chang J, *et al.* TGFβ-blockade uncovers stromal plasticity in tumors by revealing the existence of a subset of interferon-licensed fibroblasts. Nature Communications **2020**;11:6315
38. Yang Y, Yang HH, Tang B, Wu AML, Flanders KC, Moshkovich N, *et al.* The Outcome of TGFβ Antagonism in Metastatic Breast Cancer Models In Vivo Reflects a Complex Balance between Tumor-Suppressive and Proprogression Activities of TGFβ. Clinical Cancer Research **2020**;26:643-56
39. Holmgaard RB, Schaer DA, Li Y, Castaneda SP, Murphy MY, Xu X, *et al.* Targeting the TGFbeta pathway with galunisertib, a TGFbetaRI small molecule inhibitor, promotes anti-tumor immunity leading to durable, complete responses, as monotherapy and in combination with checkpoint blockade. J Immunother Cancer **2018**;6:47
40. Tauriello DVF, Palomo-Ponce S, Stork D, Berenguer-Llergo A, Badia-Ramentol J, Iglesias M, *et al.* TGFbeta drives immune evasion in genetically reconstituted colon cancer metastasis. Nature **2018**;554:538-43
41. Bremnes RM, Dønnem T, Al-Saad S, Al-Shibli K, Andersen S, Sirera R, *et al.* The Role of Tumor Stroma in Cancer Progression and Prognosis: Emphasis on Carcinoma-Associated Fibroblasts and Non-small Cell Lung Cancer. Journal of Thoracic Oncology **2011**;6:209-17
42. Joshi RS, Kanugula SS, Sudhir S, Pereira MP, Jain S, Aghi MK. The Role of Cancer-Associated Fibroblasts in Tumor Progression. Cancers (Basel) **2021**;13
43. Sinn M, Denkert C, Striefler JK, Pelzer U, Stieler JM, Bahra M, *et al.* α-Smooth muscle actin expression and desmoplastic stromal reaction in pancreatic cancer: results from the CONKO-001 study. British Journal of Cancer **2014**;111:1917-23
44. Vathiotis IA, Moutafi MK, Divakar P, Aung TN, Qing T, Fernandez A, *et al.* Alpha-smooth Muscle Actin Expression in the Stroma Predicts Resistance to Trastuzumab in Patients with Early-stage HER2-positive Breast Cancer. Clin Cancer Res **2021**;27:6156-63
45. Kawase T, Yasui Y, Nishina S, Hara Y, Yanatori I, Tomiyama Y, *et al.* Fibroblast activation protein-α-expressing fibroblasts promote the progression of pancreatic ductal adenocarcinoma. BMC gastroenterology **2015**;15:109
46. Coto-Llerena M, Ercan C, Kancherla V, Taha-Mehlitz S, Eppenberger-Castori S, Soysal SD, *et al.* High Expression of FAP in Colorectal Cancer Is Associated With Angiogenesis and Immunoregulation Processes. Front Immunol **2020**;10
47. Nissen NI, Karsdal M, Willumsen N. Collagens and Cancer associated fibroblasts in the reactive stroma and its relation to Cancer biology. Journal of experimental & clinical cancer research : CR **2019**;38:115
48. Northcott JM, Dean IS, Mouw JK, Weaver VM. Feeling Stress: The Mechanics of Cancer Progression and Aggression. Frontiers in cell and developmental biology **2018**;6:17
49. Cox TR, Bird D, Baker AM, Barker HE, Ho MW, Lang G, *et al.* LOX-mediated collagen crosslinking is responsible for fibrosis-enhanced metastasis. Cancer Res **2013**;73:1721-32
50. Horn LA, Chariou PL, Gameiro SR, Qin H, Iida M, Fousek K, *et al.* Remodeling the tumor microenvironment via blockade of LAIR-1 and TGF-β signaling enables PD-L1–mediated tumor eradication. The Journal of Clinical Investigation **2022**;132
51. Principe DR, Timbers KE, Atia LG, Koch RM, Rana A. TGFβ Signaling in the Pancreatic Tumor Microenvironment. Cancers **2021**;13:5086
52. Zhang B, Halder SK, Kashikar ND, Cho YJ, Datta A, Gorden DL, *et al.* Antimetastatic role of Smad4 signaling in colorectal cancer. Gastroenterology **2010**;138:969-80.e1-3
53. Subramanian G, Schwarz RE, Higgins L, McEnroe G, Chakravarty S, Dugar S, *et al.* Targeting Endogenous Transforming Growth Factor β Receptor Signaling in SMAD4-Deficient Human Pancreatic Carcinoma Cells Inhibits Their Invasive Phenotype. Cancer Research **2004**;64:5200-11
54. Li J, Yuan S, Norgard RJ, Yan F, Sun YH, Kim I-K, *et al.* Epigenetic and Transcriptional Control of the Epidermal Growth Factor Receptor Regulates the Tumor Immune Microenvironment in Pancreatic Cancer. Cancer Discovery **2021**;11:736-53

55. Huang H, Zhang Y, Gallegos V, Sorrelle N, Zaid MM, Toombs J*, et al.* Targeting TGFβR2-mutant tumors exposes vulnerabilities to stromal TGFβ blockade in pancreatic cancer. EMBO Mol Med **2019**;11:e10515
56. Clements DR, Sterea AM, Kim Y, Helson E, Dean CA, Nunokawa A*, et al.* Newly Recruited CD11b+, GR-1+, Ly6Chigh Myeloid Cells Augment Tumor-Associated Immunosuppression Immediately following the Therapeutic Administration of Oncolytic Reovirus. J Immunol **2015**;194:4397-412
57. Beckham JD, Tuttle K, Tyler KL. Reovirus activates transforming growth factor beta and bone morphogenetic protein signaling pathways in the central nervous system that contribute to neuronal survival following infection. J Virol **2009**;83:5035-45
58. Stanifer ML, Rippert A, Kazakov A, Willemsen J, Bucher D, Bender S*, et al.* Reovirus intermediate subviral particles constitute a strategy to infect intestinal epithelial cells by exploiting TGF-β dependent pro-survival signaling. Cellular Microbiology **2016**;18:1831-45
59. Guo L, Smith JA, Abelson M, Vlasova-St Louis I, Schiff LA, Bohjanen PR. Reovirus infection induces stabilization and up-regulation of cellular transcripts that encode regulators of TGF-β signaling. PloS one **2018**;13:e0204622-e
60. Macedo N, Miller DM, Haq R, Kaufman HL. Clinical landscape of oncolytic virus research in 2020. Journal for ImmunoTherapy of Cancer **2020**;8:e001486
61. Schneider CA, Rasband WS, Eliceiri KW. NIH Image to ImageJ: 25 years of image analysis. Nature Methods **2012**;9:671-5
62. Hawinkels LJ, Paauwe M, Verspaget HW, Wiercinska E, van der Zon JM, van der Ploeg K*, et al.* Interaction with colon cancer cells hyperactivates TGF-β signaling in cancer-associated fibroblasts. Oncogene **2014**;33:97-107

SUPPLEMENTARY METHODS

Immunohistochemistry

Formalin-fixed tumor pieces were embedded in paraffin and then sectioned randomly at 4 µm and placed on Superfrost® Plus slides (VWR). Sections were dried overnight at 37 °C and stored at 4 °C until staining. Slides were deparaffinized and endogenous peroxidase was blocked with 0,3% hydrogen peroxidase (VWR) in methanol for 20 minutes. After rehydration, antigen retrieval was performed by boiling slides for 10 minutes in 0,01M sodium citrate (pH 6) (Merck). Non-specific binding was blocked using SuperBlock™ (ThermoFisher Scientific) before overnight incubation in PBS/1% BSA in a humified box at 4 °C or RT with rabbit anti-mouse CD3ε (clone D7A6E™, 1:200; Cell Signaling Technology), rat anti-mouse CD8a (clone 4SM15, 1:1600; eBioscience™), mouse anti-mouse α-smooth muscle actin (clone 1A4/ASM-1, 1:1600/1:3200; Progen), rabbit anti-mouse phosphorylated-Smad2 (clone 138D4, 1:50; Cell Signaling Technology), rabbit anti-mouse vimentin (clone D21H3, 1:400; Cell Signaling Technology), mouse anti-mouse pan-cytokeratin (clone PCK-26, 1:400; Sigma-Aldrich) or rabbit anti-mouse Ki67 (clone SP6, 1:300, Abcam). Hereafter, samples were incubated for 30 min at RT with biotinylated goat anti-rabbit, rabbit anti-rat, or goat anti-mouse secondary antibodies (1:200; Agilent), followed by incubation with avidin-biotin complex (VECTASTAIN® Elite® ABC HRP Kit; Vector Laboratories). Peroxidase activity was detected using the 2-component liquid DAB+ system (Agilent) according to the manufacturer's instructions for 5 min. Slides were counterstained in hematoxylin (Sigma Aldrich) for 15 seconds, dehydrated, and mounted using Entellan (Sigma Aldrich). Control sections were processed in parallel, but without incubation with the primary antibody. No labeling was observed in the control sections. Collagen was stained by incubating rehydrated slides in 0.1% Sirius Red (Direct Red 80; Sigma-Aldrich) in 1.3% picric acid (Sigma-Aldrich) for 90 minutes after which slides were washed, dehydrated, and mounted as described above. αSMA, CD3, collagen, and Ki67 immunohistochemistry stainings were quantified by measuring the positive DAB or Sirius Red signal using ImageJ, and researchers analyzing the tissues were blinded to treatment groups (61).

Western Blotting

Phosphorylation of the downstream TGF-β signaling molecule Smad2 (pSmad2) in KPC3 tumor cells was analyzed by western blot as described before (62). Briefly, KPC3 cells were lysed in radioimmunoprecipitation assay (RIPA) buffer containing protease and phosphatase inhibitors using a stainless bead and the TissueLyser LT (Qiagen). Proteins (30 µg) were separated on a 10% SDS–polyacrylamide gel under reducing conditions and then transferred to a 0.45 µM PVDF membrane (Merck). After blocking for 1h at RT with 5% milk powder (Campina) in Tris-HCl-buffered saline containing 0.05% Tween-20 (TBS-T; Merck, Darmstadt, Germany), the membrane was incubated overnight at 4°C with anti-pSmad2 (Ser465/467) (clone 138D4; Cell Signaling Technology, 1:1000) or anti-β-actin (clone C4; Santa Cruz, 1:5000), followed HRP-conjugated goat anti-rabbit or anti-mouse IgG (Agilent, 1:5000) at RT for 90 minutes. After washing, proteins were

detected on the Chemidoc imaging XRS+ system (Bio-Rad) using the Clarity Western ECL Substrate kit (Bio-Rad).

TGF-β1 ELISA

Snap-frozen KPC3 or MC38 tumor pieces were lysed in radioimmunoprecipitation assay (RIPA) buffer containing protease and phosphatase inhibitors using a stain-less bead and the TissueLyser LT (Qiagen). Homogenate was centrifuged at $13x10^3$ rpm for 15 minutes at 4 °C, after which supernatants were collected and stored at −80 °C until further analysis. Active and total mTGF-β1 levels were measured by using a Mouse TGF-β1 duoset ELISA kit according to the manufacturer's instructions (R&D Systems, Minneapolis, MN, USA). Absorbance was measured using the SpectraMax iD3 multi-mode plate reader (Molecular Devices). Final values were expressed per µg protein in the tumor lysate.

CAGA-Luciferase Reporter Assay

HepG2 (RRID:CVCL_0027) is a cell line derived from a human hepatoblastoma and was obtained from ATCC (HB-8065™). $1x10^6$ HepG2 cells per well were plated into a 6-wells plate. The next days, cells were transfected with 2 µg of TGF-β/Smad inducible $(CAGA)_{12}$ luciferase transcriptional reporter construct, which encodes 12 repeats of the AGCCAGACA sequence (identified as a SMAD3/SMAD4-binding element in the human *SERPIN 1* promoter [39]) using lipofectamine 2000 transfection reagent (1:5; ThermoFisher Scientific). After overnight incubation, cells were harvested and 20.000 cells/well were plated in a 96-wells plate. After attachment, HepG2 cells were serum-starved overnight. The next day, serum-free media were removed and replaced by medium containing TGF-β1 (0.001 - 5 ng/mL, Peprotech). In other wells, TGF-β1 was added in a concentration of 5 ng/mL in combination with increasing concentrations of the monoclonal TGFβ-blocking antibody (αTGF-β) 0.01 – 10 ng/mL, BioXCell). After overnight incubation, the luciferase signal was measured using the Luciferase Assay System (Promega) according to the manufacturer's instructions using the SpectraMax iD3 multi-mode plate reader (Molecular Devices).

Lactate dehydrogenase (LDH) assay

The ability of T cells to induce killing of tumor cells was evaluated using a colorimetric method for quantifying cellular cytotoxicity. In short, KPC3.TRP1, MC38 or MC38.TRP1 cells were irradiated at 8000 RAD and plated at a concentration of 30.000 cells/well. Splenocytes and lymph nodes were isolated from either treatment-naive C57BL/6J, CD8 TGF-βRII KO, or TGF-βRII WT mice and were enriched for CD8 T cells using the Mouse CD8 T Lymphocyte Enrichment Set – DM (BD Biosciences) or via nylon wool processing. Effector cells were added to tumor cells in an E/T ratio of 10:1 and CD3-bsAbs were added in a concentration of 1 µg/mL. In the experiment with naive splenocytes from C57BL/6J mice, αTGF-β (100 or 10 µg/mL) was added as well. After 48 hours of incubation, 20 µL of Triton-X100 was added to wells containing tumor cells alone for 30 minutes to serve as a positive control. Hereafter, 50 µL of supernatant was harvested

of all conditions and incubated for 30 minutes with 50 µL of lactate dehydrogenase reaction mix (Pierce LDH Cytotoxicity Assay Kit, ThermoFisher Scientific). Absorbance was measured at 490 using a SpectraMax iD3 multi-mode plate reader (Molecular Devices). The percentage of cytotoxicity was calculated using the positive control as 100 % cytotoxicity. All conditions were performed in triplicate.

SUPPLEMENTARY FIGURES

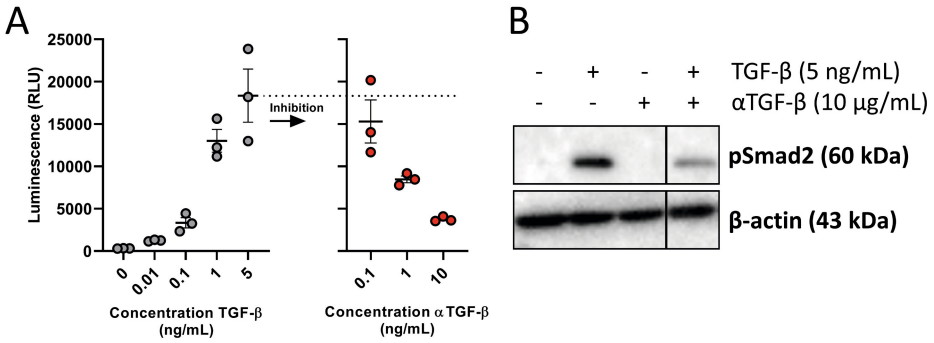

Figure S1. Inhibition of TGF-β signaling by the monoclonal antibody 1D11. (**A**) Induction of TGF-β signaling by TGF-β and subsequent inhibition of TGF-β signaling via TGF-β neutralizing antibodies (αTGF-β, 1D11), as measured by transcriptional CAGA-Luciferase reporter assay. Cells were incubated with TGF-β (0-5 ng/mL). In other wells with 5 ng/mL of TGF-β, αTGF-β was added (0.1-10 ng/mL). (**B**) Immunoblotting of phospho-Smad2 in KPC3 tumor cell line after TGF-β (5 ng/mL) and/or αTGF-β treatment (10 µg/mL). B-actin was measured as a loading control. Vertical black line indicates cutting of blot to eliminate irrelevant samples. Data represent mean±SEM.

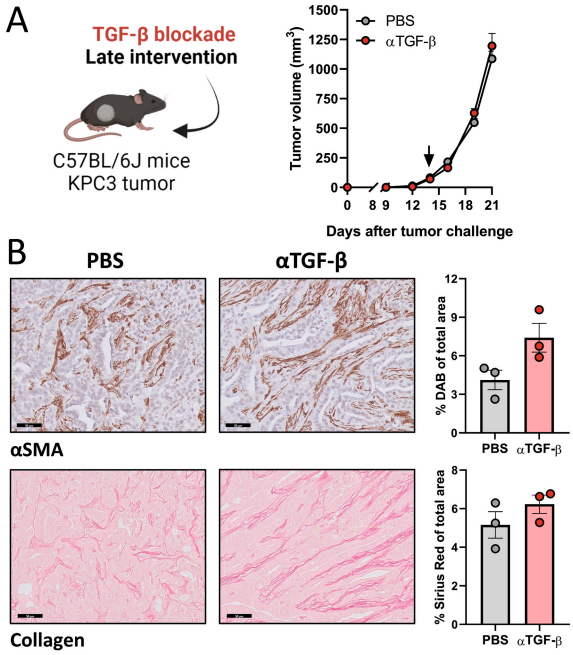

Figure S2. Late TGF-β blockade does not affect tumor outgrowth. (**A**) Average tumor growth curves of immunocompetent C57BL/6J mice (n=5/group) engrafted with KPC3 tumors (1x10^5 cells/mouse) and receiving αTGF-β (200 µg/injection every 3 days, starting on day 14, indicated by black arrow) as late intervention. (**B**) Immunohistochemistry stainings for αSMA and collagen in representative tumors after indicated treatments. Scale bars represent 50 µm and stainings were quantified using ImageJ. Data represent mean±SEM. Significance between PBS and αTGF-β was determined using unpaired t-tests.

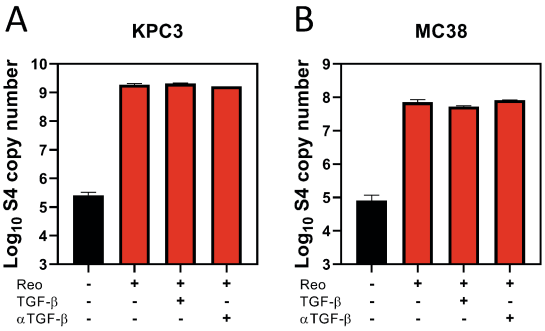

Figure S3. TGF-β addition or blockade does not affect reovirus replication in KPC3 and MC38 cells in vitro. Reovirus genomic segment 4 (S4) copy number in KPC3 (**A**) or MC38 (**B**) lysates, as determined by RT-qPCR. Cells were infected with reovirus for 24 hours (multiplicity of infection of 10) in the presence of TGF-β (5 ng/mL) or αTGF-β (10 µg/mL). Data represent mean±SEM.

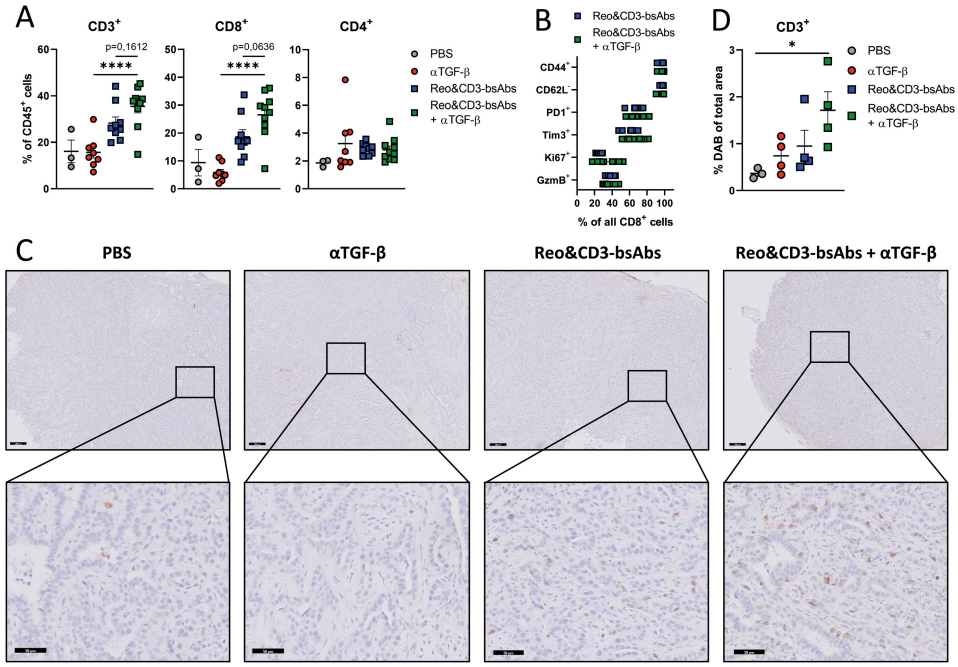

Figure S4. TGF-β blockade does not impair Reo&CD3-bsAb efficacy by decreasing T-cell influx or activation. (**A**) Frequency of $CD3^+$, $CD8^+$ and $CD4^+$ T cells within the total $CD45^+$ immune cell population in end-stage tumors after indicated treatments. (**B**) Expression of various markers on intratumoral CD8+ T cells after receiving Reo&CD3-bsAbs or Reo&CD3-bsAb + αTGF-β. (**C**) Immunohistochemistry staining for CD3 in representative tumors after indicated treatments. Scale bars represent 200 µm for overview and 50 µm for magnification, respectively. (**D**) Quantification of positive DAB signal in tumor coupes stained for CD3 after receiving indicated treatments. Data represent mean±SEM. Significance between groups in (A) and (D) was determined using an ordinary one-way ANOVA with Tukey's multiple comparisons test. Significance levels: ns=not significant, *p<0.05 and **p<0.01.

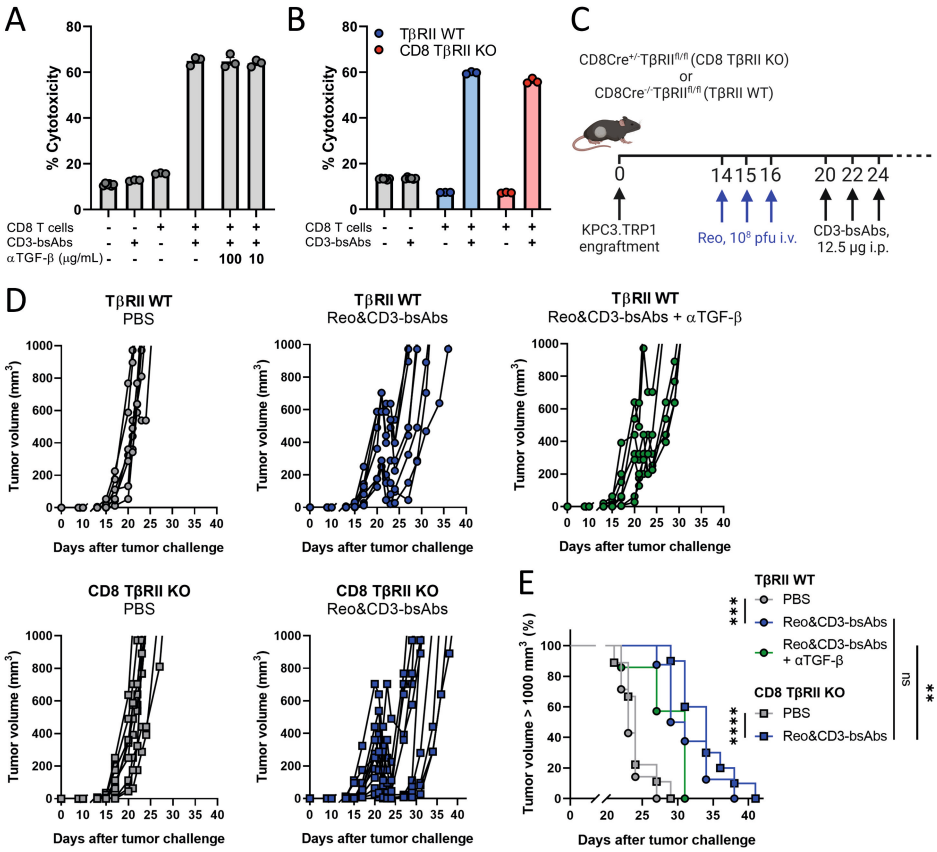

Figure S5. CD8-specific TGF-β blockade does not impair the efficacy of Reo&CD3-bsAb therapy. (**A**) Percentages of cytotoxicity of KPC3.TRP1 cells after in vitro co-culture with enriched $CD8^+$ T cells from naive mice and CD3-bsAbs, in combination with TGF-β neutralizing antibodies. (**B**) Percentage of cytotoxicity of KPC3.TRP1 cells after in vitro co-culture with enriched $CD8^+$ T cells from TβRII WT or CD8 TβRII KO mice and CD3-bsAbs. Data represents mean±SEM of triplicates. (**C**) Overview of the experiment described in (B-C). TβRII or CD8 TβRII KO mice (n=7-10/group) were subcutaneously engrafted with KPC3.TRP1 cells ($1x10^5$/mouse). Mice received Reo intravenously on days 14, 15, and 16 (10^8 plaque-forming units/injection) and received CD3-bsAbs intraperitoneally (12.5 μg/injection) on days 20, 22, and 24. Tumor growth was measured 3-5x/week. (**D**) Individual tumor growth curves of mice receiving indicated treatments. (**E**) Kaplan-Meier survival graphs of mice after indicated treatments. Log-rank tests were used to compare differences in survival in (E). Significance levels: ns= not significant, **p<0.01, ***p<0.001 and ****p<0.0001.

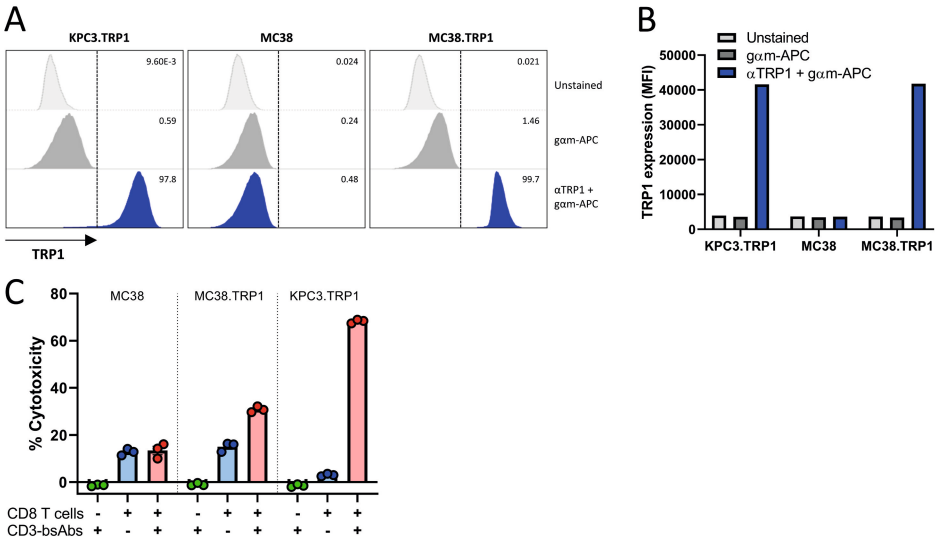

Figure S6. Introduction of TRP1 expression on MC38.TRP1 cells allows killing via CD3-bsAbs. (**A**) Percentage of TRP1 expression on MC38 cells after transfection and sorting, as measured by flow cytometry. Non-transfected MC38 cells are used as negative control and KPC3.TRP1 cells act as a positive control. (**B**) Comparison of mean fluorescence intensity (MFI) of TRP1 signal between KPC3.TRP1 and MC38.TRP1. (**C**) Percentages of cytotoxicity of KPC3.TRP1, MC38 and MC38.TRP1 cells after in vitro co-culture with nylon-wool enriched T cells from naive mice and CD3-bsAbs. Data represents mean±SEM of triplicates.

SUPPLEMENTARY TABLES

Table S1. List of antibodies used for flow cytometric analysis.

Marker	*Clone*	*Fluorochrome*	*Supplier*
CD45.2	104	FITC	eBioscience
CD3	145-2C11	PE-CF594	BD Biosciences
CD8α	53-6.7	Alexa Fluor 700	eBioscience
CD4	RM4-5	APC	BioLegend
Reo $\mu1_{133-140}$ Tetramer		APC	In-house
Rpl18 Tetramer		PE	In-house
CD44	IM-7	BV785	BioLegend
CD62L	MEL-14	BV421	BioLegend
PD-1	29F.1A12	APC-Cy7	BioLegend
Tim3	RMT3-23	PE	BioLegend
NKG2A	16A11	PE	eBioscience
KLRG-1	2F1	PE-Cy7	eBioscience
CD69	H1.2F3	BV605	BioLegend
Lag3	C9B7W	PE-Cy7	Invitrogen
CD49a	Ha31/8	BV786	BD Biosciences
CD103	2E7	BV711	BioLegend
Ki67	B56	BV711	BD Biosciences
GzmB	NGZB	PE-Cy7	BioLegend

Table S2. List of primers used for RT-qPCR analysis.

Gene	*Forward*	*Reverse*
S4Q	5′-CGCTTTTGAAGGTCGTGTATCA-3′	5′-CTGGCTGTGCTGAGATTGTTTT-3′
Ifit-1	5′-CTGGACAAGGTGGAGAAGGT-3′	5′-AGGGTTTTCTGGCTCCACTT-3′
Ifit-2	5′-TGCTCTTGACTGTGAGGAGG-3′	5′-ATCCAGACGGTAGTTCGCAA-3′
Ifit-3	5′-GTGCAACCAGGTCGAACATT-3′	5′- AGGTGACCAGTCGACGAATT-3′
Irf7	5′-GACCGTGTTTACGAGGAACC-3′	5′-GCTGTACAGGAACACGCATC-3′
Isg15	5′-GGAACGAAAGGGGCCACAGCA-3′	5′-CCTCCATGGGCCTTCCCTCGA-3′
Oas1b	5′-AGCATGAGAGACGTTGTGGA-3′	5′-GCGTAGAATTGTTGGTTAGGCT-3′
Ddx58	5′-AAGGCCACAGTTGATCCAAA-3′	5′-TTGGCCAGTTTTCCTTGTCG-3′
Cxcl9	5′-TGGAGTTCGAGGAACCCTAGT-3′	5′-AGGCAGGTTTGATCTCCGTT-3′
Cxcl10	5′-ACGAACTTAACCACCATCT-3′	5′-TAAACTTTAACTACCCATTGATACATA-3′
Mx1	5′-GATGGTCCAAACTGCCTTCG-3′	5′-TTGTAAACCTGGTCCTGGCA-3′
β2m	5′-CTCGGTGACCCTGGTCTTT-3′	5′-CCGTTCTTCAGCATTTGGAT-3′
Bst2	5′-ACATGGCGCCCTCTTTCTATCACT-3′	5′-TGACGGCGAAGTAGATTGTCAGGA-3′
Rsad2	5′-GGTGCCTGAATCTAACCAGAAG-3′	5′-CCACGCCAACATCCAGAATA-3′
Ctgf	5′-GGCCTCTTCTGCGATTTCG-3′	5′-CCATCTTTGGCAGTGCACACT-3′
Id-1	5′-ACCCTGAACGGCGAGATCA-3′	5′-TCGTCGGCTGGAACACAT-3′
Mmp2	5′-TTCTGTCCCGAGACCGCTAT-3′	5′-GTGTAGATCGGGGCCATCAG-3′

Table S2. Continued.

Gene	*Forward*	*Reverse*
Serpin E1	5′-GCCAACAAGAGCCAATCACA-3′	5′-AGGCAAGCAAGGGCTGAAG-3′
Snail	5′-AGCCCAACTATAGCGAGCTG-3′	5′-CCAGGAGAGAGTCCCAGATG-3′
TGF-β1	5′-CAACAATTCCTGGCGTTACC-3′	5′-TGCTGTCACAAGAGCAGTGA-3′
Mzt2	5′-TCGGTGCCCATATCTCTGTC-3′	5′-CTGCTTCGGGAGTTGCTTTT-3′
Ptp4a2	5′-AGCCCCTGTGGAGATCTCTT-3′	5′-AGCATCACAAACTCGAACCA-3′